Neuron

Article

The Calmodulin-interacting peptide Pcp4a regulates feeding state-dependent behavioral choice in zebrafish

Graphical abstract

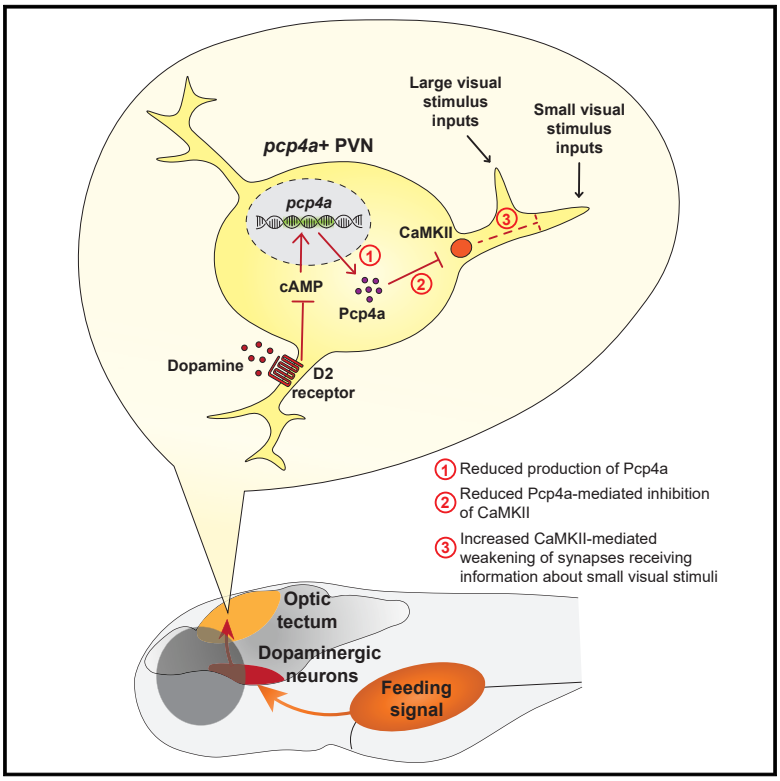

Highlights

- Food intake regulates production of the intracellular peptide Pcp4a in the brain
- Pcp4a modulates behavioral choice in an approach/avoidance assay
- Pcp4a controls visual size tuning of *pcp4a*+ neurons in the tectum
- The dopaminergic system modulates visual response properties of tectal *pcp4a*+ neurons

Authors

Margherita Zaupa, Nagarjuna Nagaraj, Anna Sylenko, Herwig Baier, Suphansa Sawamiphak, Alessandro Filosa

Correspondence

alessandro.filosa@mdc-berlin.de

In brief

Zaupa et al. identify the intracellular peptide Pcp4a as a mediator of the modulatory action of feeding state on behavioral choice. Food intake represses expression of *pcp4a* via activation of dopamine D2 receptors, leading to disinhibition of CaMKII and possibly increased CaMKII-dependent weakening of responses to small visual stimuli.

Zaupa et al., 2024, Neuron *112*, 1–15
April 3, 2024
https://doi.org/10.1016/j.neuron.2024.01.001

CellPress

Neuron

CellPress
OPEN ACCESS

Article

The Calmodulin-interacting peptide Pcp4a regulates feeding state-dependent behavioral choice in zebrafish

Margherita Zaupa,[1,2] Nagarjuna Nagaraj,[3,5] Anna Sylenko,[1,2] Herwig Baier,[4] Suphansa Sawamiphak,[1] and Alessandro Filosa[1,6,*]

[1]Max Delbrück Center for Molecular Medicine in the Helmholtz Association (MDC), 13092 Berlin, Germany
[2]Freie Universität Berlin, Institute for Biology, 14195 Berlin, Germany
[3]Biochemistry Core Facility, Max Planck Institute of Biochemistry, 82152 Martinsried, Germany
[4]Max Planck Institute for Biological Intelligence, 82152 Martinsried, Germany
[5]Present address: Evotec München GmbH, 82061 Neuried, Germany
[6]Lead contact
*Correspondence: alessandro.filosa@mdc-berlin.de
https://doi.org/10.1016/j.neuron.2024.01.001

SUMMARY

Animals constantly need to judge the valence of an object in their environment: is it potential food or a threat? The brain makes fundamental decisions on the appropriate behavioral strategy by integrating external information from sensory organs and internal signals related to physiological needs. For example, a hungry animal may take more risks than a satiated one when deciding to approach or avoid an object. Using a proteomic profiling approach, we identified the Calmodulin-interacting peptide Pcp4a as a key regulator of foraging-related decisions. Food intake reduced abundance of protein and mRNA of *pcp4a* via dopamine D2-like receptor-mediated repression of adenylate cyclase. Accordingly, deleting the *pcp4a* gene made zebrafish larvae more risk averse in a binary decision assay. Strikingly, neurons in the tectum became less responsive to prey-like visual stimuli in *pcp4a* mutants, thus biasing the behavior toward avoidance. This study pinpoints a molecular mechanism modulating behavioral choice according to internal state.

INTRODUCTION

To live and thrive in complex environments, animals and humans have to make decisions to select optimal behaviors in response to external stimuli and internal needs. Internal states have a strong influence on decision-making.[1–4] For example, hunger can increase the propensity to take risks and to tolerate aversive stimuli.[5–10] Moreover, metabolic state can modulate processing of sensory cues influencing decision-making. In rodents, non-human primates, and humans, hunger enhances responses to images of food in several cortical areas involved in visual processing and in structures of the limbic system such as the amygdala.[11–15] Modulation of sensory processing may represent an efficient way to bias behavioral selection processes, which need to be fast for ensuring an animal's survival, such as deciding to escape or not from potential danger.[16]

While some progress has been made in identifying the brain regions and neuronal circuits mediating the effect of internal states on decision-making,[17–20] the molecular mechanisms orchestrating the actions of these circuits are still largely unknown.[17] Indeed, although several neurotransmitter systems have been implicated in modulating decision-making,[17,21] little is known about the downstream molecular machinery. This current situation is in stark contrast to the very detailed knowledge of molecular events regulating other cognitive functions such as learning and memory.[22]

Here, we used zebrafish larva as a model organism to identify molecular regulators of action selection. Zebrafish larvae display several well-characterized motor behaviors, some of which are modulated by internal states.[23] For example, they approach small moving visual stimuli simulating natural prey, such as rotifers and paramecia,[24–26] and avoid larger ones resembling approaching predators.[27,28] While stimulus size is an important factor dictating whether a fish will approach or avoid a visual stimulus,[24,26,29] internal states also play a crucial role in this decision. Indeed, we previously found that feeding state in zebrafish is a strong regulator of behavioral choice.[30] Food-deprived fish take more risks when deciding to approach or avoid ambiguous prey-sized visual stimuli, compared with fed animals. Moreover, small visual stimuli resembling prey are overrepresented in the tectum of food-deprived fish, a midbrain region critically involved in regulating prey capture and avoidance behaviors in zebrafish.[27,28,31–33] Now we have identified the intracellular peptide Pcp4a as an essential

Please cite this article in press as: Zaupa et al., The Calmodulin-interacting peptide Pcp4a regulates feeding state-dependent behavioral choice in zebrafish, Neuron (2024), https://doi.org/10.1016/j.neuron.2024.01.001

component of the molecular machinery regulating neuronal changes underlying feeding-state-dependent behavioral choice in zebrafish.

Pcp4a is homologous to the mammalian peptide PCP4 (also known as PEP-19), which inhibits the function of Calmodulin,[34,35] a calcium-binding protein regulating neuronal excitability and synaptic plasticity.[36,37] Accordingly, mice lacking PCP4 have altered cerebellar synaptic plasticity.[38] Moreover, *pcp4a* in zebrafish larvae is expressed in the tectum.[39] We found that food intake represses expression of *pcp4a* in the brain. Correspondingly, food-deprived *pcp4a* mutant fish behave similarly to fed ones in an approach/avoidance decision assay, and their tectal neurons are less responsive to prey-like visual stimuli, like in fed fish. We also found that expression of *pcp4a* is repressed by the dopaminergic system through dopamine D2-like receptor-mediated inhibition of adenylate cyclase. Fittingly, activation of D2-like receptors induces changes of visual size representation in the tectum similar to the ones present in *pcp4a* mutants. Together, our findings point to Pcp4a as a critical regulator of neuronal physiology underlying modulation of behavioral choice guided by internal states.

RESULTS

Food intake regulates transcription of *pcp4a* in the brain

To understand how feeding state regulates behavioral selection at the molecular level, we performed mass spectrometry analysis to compare the proteomes of food-deprived and fed larvae. With this approach, we identified 166 proteins displaying statistically significant differential abundance in fed versus food-deprived 7 days post-fertilization (dpf) wild-type (WT) larvae (Figure 1A; Table S1). These proteins are involved in several biological processes, including metabolic functions, interaction with nucleic acids, signal transduction, endocytosis/exocytosis, and regulation of cell cycle (Table S1). When choosing candidates for functional validation, we decided to focus on proteins known to regulate neuronal excitability and/or synaptic function and to be expressed in the zebrafish tectum. An outstanding candidate fulfilling these criteria was the peptide Pcp4a, which was 35% less abundant in fed compared with food-deprived fish (Figure 1B; Table S1). Since PCP4 was shown to regulate synaptic plasticity and potentially neuronal excitability via modulation of Calmodulin's activity,[34,35,38] and considering the fact that *pcp4a* is expressed in the tectum and few other regions of the central nervous system of zebrafish larvae[39] (Figures 1C and S1), we decided to further explore a potential role of Pcp4a in regulating behavioral choice according to feeding state. We first tested if regulation of Pcp4a abundance by feeding state happens specifically in the brain. To this end, we measured amounts of *pcp4a*'s mRNA in the brains of 7 dpf food-deprived and fed larvae using real-time quantitative reverse-transcription polymerase chain reaction (RT-qPCR). In agreement with our mass spectrometry results, we found that *pcp4a* expression was lower in fed fish than in unfed ones (Figure 1D).

Together, these results indicate that food intake reduces abundance of Pcp4a in the brain, through a mechanism regulating transcription of its mRNA.

Lack of Pcp4a alters behavioral choice

We next tested whether Pcp4a could influence behavioral choice, by mutating the *pcp4a* locus using the CRISPR-Cas9 technique. We identified a mutation leading to a reading frameshift and formation of an early stop codon before the sequence coding for the Calmodulin-binding domain (Figure 2A).

We employed an approach/avoidance decision assay in which a larva is confronted with visual stimuli shown from below in the form of small or large black circles on a white background, simulating a prey or a predator, respectively[29,30] (Figure 2B). We used the valence index to quantify the tendency of larvae to approach (positive valence) or avoid (negative valence) a stimulus of a certain size[29,30] (Figure 2C). The valence index ranges from −1 (if only avoidances are performed) to +1 (if only approaches are performed), and it is equal to zero when larvae pursue or avoid visual stimuli with a 50% probability. It is important to note that in this assay the small visual stimuli, although resembling potential food, are not perfect imitations of prey and may be perceived ambiguously by fish. Indeed, this type of stimuli is able to induce both approaches and avoidances.[29,30] This characteristic makes this assay ideal for testing modulatory effects on behavioral choice. We previously found that fed larvae have a more negative valence index for small circles, compared with food-deprived ones, suggesting a more conservative strategy when interacting with approaching visual stimuli.[30] Since amounts of Pcp4a are lower in fed larvae (Figures 1B and 1D), we reasoned that if Pcp4a is involved in regulating approach/avoidance decisions, food-deprived *pcp4a*$^{md78/md78}$ fish may phenocopy fed larvae. Indeed, we observed that 7 dpf *pcp4a*$^{md78/md78}$ fish displayed a more negative valence index for small visual stimuli, compared with control food-deprived WTs (Figure 2C). On the other hand, we did not detect differences of valence index between fed *pcp4a*$^{md78/md78}$ and fed WT fish (Figure S2A), suggesting that mutating *pcp4a* does not enhance the effect of food intake in the decision assay. Unfed *pcp4a* mutants displayed increased probability of avoidance of small circles and same approach probability, compared with unfed WTs (Figure 2D), indicating that the reduction of valence index in the mutants is due to an increased propensity to avoid visual stimuli.

To rule out the possibility that the *pcp4a*^{md78} mutation could lead to generalized problems in sensory-motor transformations, we also measured the probability of a fish to react to visual stimuli in the approach/avoidance decision assay, using the activity index (Figure 2E), which ranges from 0 (no interactions with stimuli) to 1 (when fish react to stimuli by approaching or avoiding them 100% of times). We found that *pcp4a*$^{md78/md78}$ fish, either fed or unfed, had unaltered probability of interaction with the visual stimuli, compared with WT controls (Figures 2E and S2B). Moreover, *pcp4a*$^{md78/md78}$ larvae did not display reduction of numbers of active interactions (Figure S2D), nor did they display impairment of spontaneous locomotion (Figures 2F and S2C) and optomotor response (Figures S2E–S2G), compared with WT fish. These results suggest that *pcp4a*$^{md78/md78}$ fish do not have generalized visual processing or motor impairments.

Taken together, these data indicate that Pcp4a regulates a decision-making process strongly modulated by feeding state.

Please cite this article in press as: Zaupa et al., The Calmodulin-interacting peptide Pcp4a regulates feeding state-dependent behavioral choice in zebrafish, Neuron (2024), https://doi.org/10.1016/j.neuron.2024.01.001

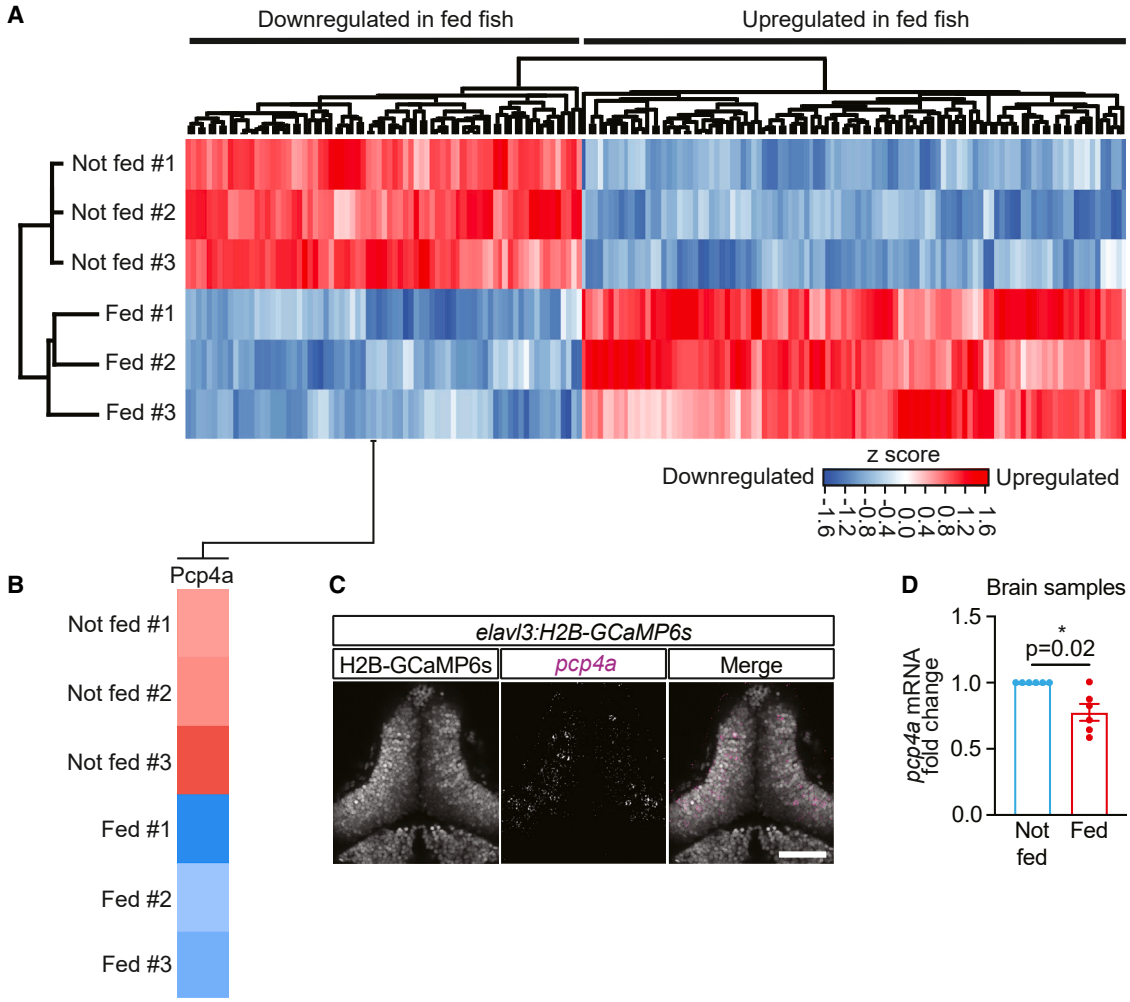

Figure 1. Feeding decreases abundance of Pcp4a

(A) Heatmap with dendrogram of hierarchical clustering of proteins significantly (FDR < 0.05) differentially abundant in fed and not-fed 7 dpf wild-type larvae. Three biological replicas (pool of ten larvae each) were used for each feeding condition.

(B) An enlarged detail from the heatmap in (A), showing Pcp4a reduced abundance in fed larvae.

(C) Confocal images of the tectum of a 7 dpf *elavl3:H2B-GCaMP6s* larva, showing nuclei of neurons labeled with GCaMP6s and *pcp4a*'s mRNA localization. Scale bars, 50 μm.

(D) Bar graph depicting fold change of *pcp4a*'s mRNA levels (in fed versus not-fed fish) in the brain of 7 dpf wild-type larvae. n = 6 for each condition. n indicates number of biological replicas (ten pooled brains per each replica). Statistical significance was determined with one-sample t test. Data are shown as mean ± standard error of the mean.

See also Figure S1 and Table S1.

Pcp4a modulates responses to visual stimuli in the tectum

We previously showed that food intake shifts population responses of periventricular neurons (PVNs) in the tectum toward large (predator-like) visual stimuli at the expense of responses to small (prey-like) stimuli.[30] Since *pcp4a* is expressed by a fraction of PVNs at 7 dpf (Figures 1C and 3E), we hypothesized that their activity may be modulated by feeding state. To prove this, we performed calcium imaging in the tectum of 7 dpf *elavl3:H2B-GCaMP6s* larvae in which the majority of neurons in the brain contain the nucleus-targeted, genetically encoded calcium indicator GCaMP6s[40] (Figure 3A). To identify *pcp4a*-positive (*pcp4a*+) neurons we performed post-mortem fluorescence *in situ* hybridization chain reaction (HCR)[41] after *in vivo* calcium imaging to detect localization of *pcp4a*'s mRNA. We first recorded responses of tectal PVNs to black circles of various sizes presented to the larvae on a small screen positioned on one side of the fish (Figure 3B). We quantified the size tuning of each neuron with a weighted sum of visual stimulus sizes (measured as degree of visual angle) eliciting a neuronal response, with weights corresponding to normalized ΔF/F values of each response, which we termed weighted mean response (WMR) angle (see Filosa et al.[30] and STAR Methods for a detailed explanation). We then fixed the larvae, performed *in situ* HCR to detect

Please cite this article in press as: Zaupa et al., The Calmodulin-interacting peptide Pcp4a regulates feeding state-dependent behavioral choice in zebrafish, Neuron (2024), https://doi.org/10.1016/j.neuron.2024.01.001

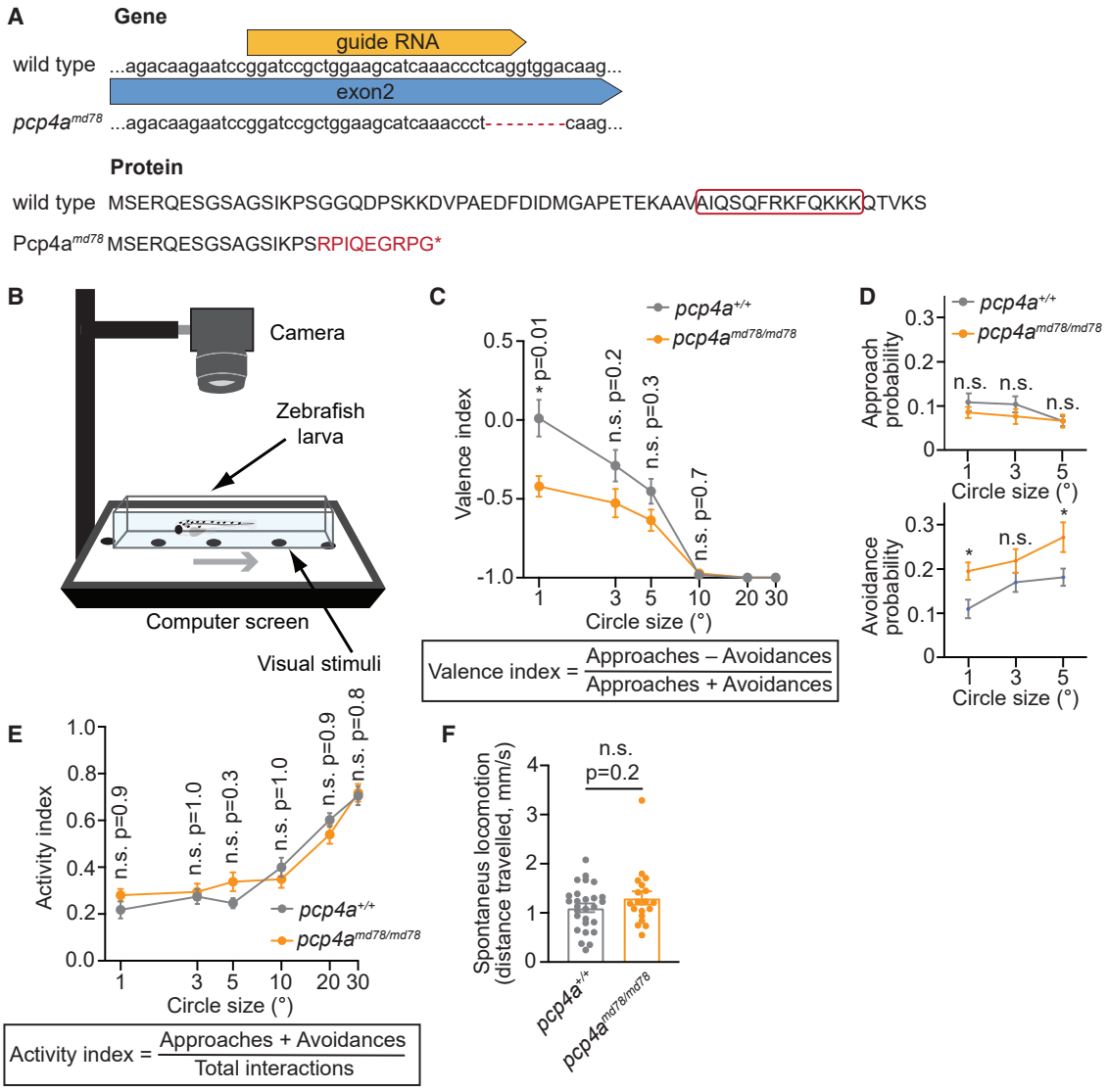

Figure 2. Mutating *pcp4a* alters decision to approach or avoid small visual stimuli

(A) Schematic representation of the strategy for mutating the *pcp4a* gene using the CRISPR-Cas9 technique. The truncated protein, if produced, would lack the Calmodulin-interacting domain (red box in the wild-type protein sequence).

(B) Scheme of the behavioral setup for recording approach/avoidance decisions of zebrafish larvae.

(C) Graph depicting average valence indexes for different sizes of visual stimuli of 7 dpf unfed *pcp4a*$^{+/+}$ and *pcp4a*$^{md78/md78}$ larvae.

(D) Graphs showing approach (top) or avoidance (bottom) probability for small visual stimuli in 7 dpf unfed *pcp4a*$^{+/+}$ and *pcp4a*$^{md78/md78}$ larvae. Approach and avoidance probabilities were calculated as (approaches/[approaches + avoidances + neutral interactions]) or (avoidances/[approaches + avoidances + neutral interactions]), respectively. For approach probability, p = 0.7 (1°), p = 0.9 (3°), and p = 1.0 (5°). For avoidance probability, p = 0.02 (1°), p = 0.2 (3°), and p = 0.04 (5°).

(E) Graph depicting average activity indexes for different sizes of visual stimuli of 7 dpf unfed *pcp4a*$^{+/+}$ and *pcp4a*$^{md78/md78}$ larvae. In (C)–(E), $n_{pcp4a+/+}$ = 22 larvae, $n_{pcp4amd78/md78}$ = 18 larvae. *p < 0.05; n.s., not significant; two-tailed t test with Bonferroni-Holm correction. (F) Bar graph showing average spontaneous locomotion of 7 dpf unfed *pcp4a*$^{+/+}$ and *pcp4a*$^{md78/md78}$ larvae. $n_{pcp4a+/+}$ = 27 larvae, $n_{pcp4amd78/md78}$ = 19 larvae. n.s., not significant; two-tailed t test. Data in (C)–(F) are shown as mean ± standard error of the mean.

See also Figure S2.

pcp4a's mRNA (which was detectable also in *pcp4a*$^{md78/md78}$ larvae, likely due to lack or incomplete mutation-induced degradation of the transcript, allowing us to classify PVNs as *pcp4a*+ and *pcp4a*− also in *pcp4a*$^{md78/md78}$ fish), and finally aligned the images of *in vivo* calcium imaging with the ones of the stained fish (using the *in vivo* GCaMP6s signal and the residual signal of GCaMP6s in the fixed larvae for the alignment) to classify each neuron responding to visual stimuli as *pcp4a*+ or *pcp4a*− (Figures 3B, 3C, and S3; STAR Methods, for a detailed explanation). In accord with our hypothesis, we found that the population response profile of *pcp4a*+ neurons was shifted toward larger circle sizes in fed larvae, compared with food-deprived ones

Please cite this article in press as: Zaupa et al., The Calmodulin-interacting peptide Pcp4a regulates feeding state-dependent behavioral choice in zebrafish, Neuron (2024), https://doi.org/10.1016/j.neuron.2024.01.001

CellPress
OPEN ACCESS

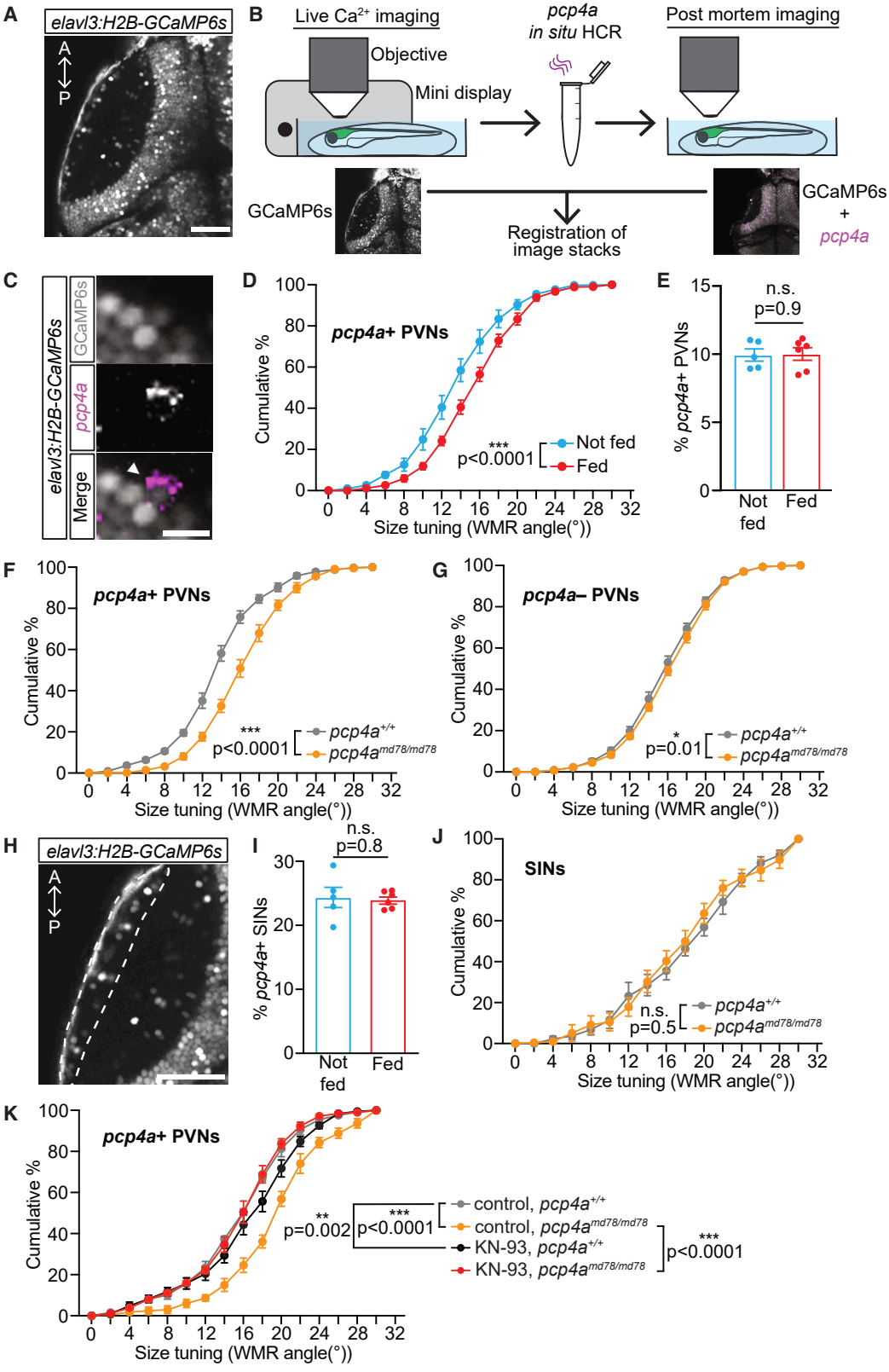

(legend on next page)

Please cite this article in press as: Zaupa et al., The Calmodulin-interacting peptide Pcp4a regulates feeding state-dependent behavioral choice in zebrafish, Neuron (2024), https://doi.org/10.1016/j.neuron.2024.01.001

(Figure 3D). A similar shift was observed also in *pcp4a*− neurons (Figure S4A), indicating that the effect of food intake is not restricted only to PVNs expressing *pcp4a*. The percentage of *pcp4a*+ tectal PVNs and their fraction responding to the visual stimuli were not altered by feeding state (Figures 3E and S4B), indicating that food intake does not control differentiation of *pcp4a*+ PVNs or their general responsiveness to visual stimuli.

Since abundance of Pcp4a is reduced by food intake, we proceeded to test whether mutating *pcp4a* in food-deprived fish would phenocopy the effect of feeding on representation of visual stimuli in the tectum, by performing calcium imaging of 7 dpf food-deprived *elavl3:H2B-GCaMP6s; pcp4a*$^{md78/md78}$ and control food-deprived *elavl3:H2B-GCaMP6s; pcp4a*$^{+/+}$ larvae. In accord with this hypothesis, we found that in homozygous *pcp4a* mutants, the response profile was shifted toward large visual stimuli (Figure 3F). Interestingly, this effect was mainly limited to *pcp4a*+ neurons since the response profile of *pcp4a*− neurons was negligibly altered by the mutation in the *pcp4a* locus (Figure 3G). PVNs in fed *pcp4a*$^{md78/md78}$ fish also displayed a small shift of responses toward large visual stimuli, compared with PVNs in fed *pcp4a*$^{+/+}$ larvae (Figure S4C), suggesting that the reduction of Pcp4a abundance that we observed in fed fish does not have a saturation effect on modulation of visual response properties of *pcp4a*+ PVNs. However, this residual effect is likely too small to have an impact on behavior (Figure S2A). The percentage of *pcp4a*+ PVNs responsive to visual stimuli were similar in *pcp4a*$^{md78/md78}$ and *pcp4a*$^{+/+}$ fish (Figure S4D), suggesting that the *pcp4a*^{md78} mutation does not alter in a generalized way the physiology of PVNs.

Superficial interneurons (SINs) present at the outer edge of the tectal neuropil were shown to control size selectivity of tectal PVNs.[42,43] Interestingly, we found that a small percentage of SINs express *pcp4a* (Figures 3H and 3I). We therefore wondered whether size tuning of SINs is altered by the *pcp4a*^{md78} mutation. However, we found that size tuning (Figure 3J) and percentage of SINs responsive to visual stimuli (Figure S4E) were not significantly different in *pcp4a*$^{md78/md78}$ fish, compared with *pcp4a*$^{+/+}$ controls.

Since pcp4a is expressed in the retina,[39] including in a small population of retinal ganglion cells (RGCs; Figures S1C and S1D), to rule out a role of Pcp4a in regulating responses of RGCs to the visual stimuli utilized in our experiments, we performed calcium imaging of axons of RGCs in the tectal neuropil of food-deprived 7 dpf *atoh7:gal4; UAS:GCaMP6s; pcp4a*$^{md78/md78}$ and *atoh7:gal4; UAS:GCaMP6s; pcp4a*$^{+/+}$ larvae (Figure S4F). *pcp4a*$^{md78/md78}$ fish did not display significant alterations of responses to the visual stimuli in the axons of RGCs (Figures S4G and S4H). These data, together with the fact that size tuning of SINs and *pcp4a*− tectal PVNs were not altered in mutant fish, suggest that Pcp4a regulates size tuning in PVNs in a cell-autonomous way.

It was shown that the mammalian PCP4, by interacting with Calmodulin, can inhibit the enzyme Ca^{2+}/calmodulin-dependent kinase II (CaMKII),[34] an important regulator of synaptic function and plasticity.[37,44] We therefore hypothesized that CaMKII activity could be elevated in *pcp4a* mutant fish, and inhibiting CaMKII could revert the shift toward large visual stimuli observed in mutant fish. To test this hypothesis, we used the CaMKII inhibitor KN-93.[45] Application of KN-93 to 7 dpf unfed *elavl3:H2B-GCaMP6s; pcp4a*$^{md78/md78}$ fish abolished the shift of visual size responses in *pcp4a*+ PVNs observed in *elavl3:H2B-GCaMP6s; pcp4a*$^{md78/md78}$ larvae treated with a control solution (Figure 3K). KN-93 did not induce a shift of responses toward smaller visual stimuli in WT fish (Figure 3K), suggesting that the amount of Pcp4a present in PVNs of unfed fish is sufficient to fully inhibit the CaMKII-mediated effect on size tuning modulation.

The serotonergic and dopaminergic systems control expression of *pcp4a*

We next wanted to identify neurotransmitter systems able to regulate expression of *pcp4a*. We first focused our attention on the serotonergic system, as we previously showed that it regulates approach/avoidance decisions and filtering of visual stimuli in the tectum.[30] Since we found that serotonergic neurons in the raphe nucleus are more active in food-deprived larvae and that enhancing serotonergic transmission in fed fish phenocopies

Figure 3. Pcp4a modulates representation of visual stimuli size in the tectum

(A) Image showing part of the tectum of a 7 dpf *elavl3:H2B-GCaMP6s* fish.

(B) Scheme of the strategy used to identify *pcp4a*+ neurons with *in situ* HCR after *in vivo* calcium imaging.

(C) Confocal images showing localization in a 7 dpf *elavl3:H2B-GCaMP6s* larva of *pcp4a*'s mRNA and GCaMP6s signal acquired during *in vivo* Ca^{2+} imaging. The images were taken from the image stack obtained after aligning the *in vivo* and post-mortem stacks.

(D) Graph depicting cumulative percentages of WMR angles of *pcp4a*+ PVNs in food-deprived and fed 7 dpf *elavl3:H2B-GCaMP6s* larvae. n_{fed} = 6 fish, $n_{not\text{-}fed}$ = 5 fish.

(E) Bar graph showing average percentages of *pcp4a*+ PVNs in fed (n = 6 fish) and not-fed (n = 5 fish) larvae.

(F and G) Graphs depicting cumulative percentages of WMR angles of *pcp4a*+ (F) or *pcp4a*− (G) PVNs in unfed 7 dpf *elavl3:H2B-GCaMP6s; pcp4a*$^{+/+}$ and *elavl3:H2B-GCaMP6s; pcp4a*$^{md78/md78}$ larvae. $n_{pcp4a+/+}$ = 6 fish, $n_{pcp4amd78/md78}$ = 6 fish.

(H) Confocal image showing SINs in the tectum of a 7 dpf *elavl3:H2B-GCaMP6s* larva. The dashed white line demarcates the neuropil region containing SINs.

(I) Bar graph showing average percentages of *pcp4a*+ SINs in fed (n = 6 fish) and not-fed (n = 5 fish) larvae.

(J) Graph depicting cumulative percentages of WMR angles of SINs in food-deprived 7 dpf *elavl3:H2B-GCaMP6s; pcp4a*$^{+/+}$ and *elavl3:H2B-GCaMP6s; pcp4a*$^{md78/md78}$ larvae. $n_{pcp4a+/+}$ = 6 fish, $n_{pcp4amd78/md78}$ = 6 fish.

(K) Graph depicting cumulative percentages of WMR angles of *pcp4a*+ PVNs in food-deprived 7 dpf *elavl3:H2B-GCaMP6s; pcp4a*$^{+/+}$ and *elavl3:H2B-GCaMP6s; pcp4a*$^{md78/md78}$ larvae, treated with the CaMKII inhibitor KN-93 or control solution. $n_{control\_pcp4a+/+}$ = 5 fish, $n_{control\_pcp4amd78/md78}$ = 4 fish, $n_{KN\text{-}93\_pcp4a+/+}$ = 6 fish, $n_{KN\text{-}93\_pcp4amd78/md78}$ = 6 fish. *p < 0.05, **p < 0.01, and ***p < 0.001; n.s., not significant; two-tailed t test (E and I) or two-way ANOVA (D, F, G, J, and K). Data are presented as mean ± standard error of the mean. Scale bars, 50 μm in (A) and (H) and 10 μm in (C). In (A) and (H), A and P indicate anterior and posterior directions, respectively.

See also Figures S3 and S4.

Please cite this article in press as: Zaupa et al., The Calmodulin-interacting peptide Pcp4a regulates feeding state-dependent behavioral choice in zebrafish, Neuron (2024), https://doi.org/10.1016/j.neuron.2024.01.001

CellPress
OPEN ACCESS

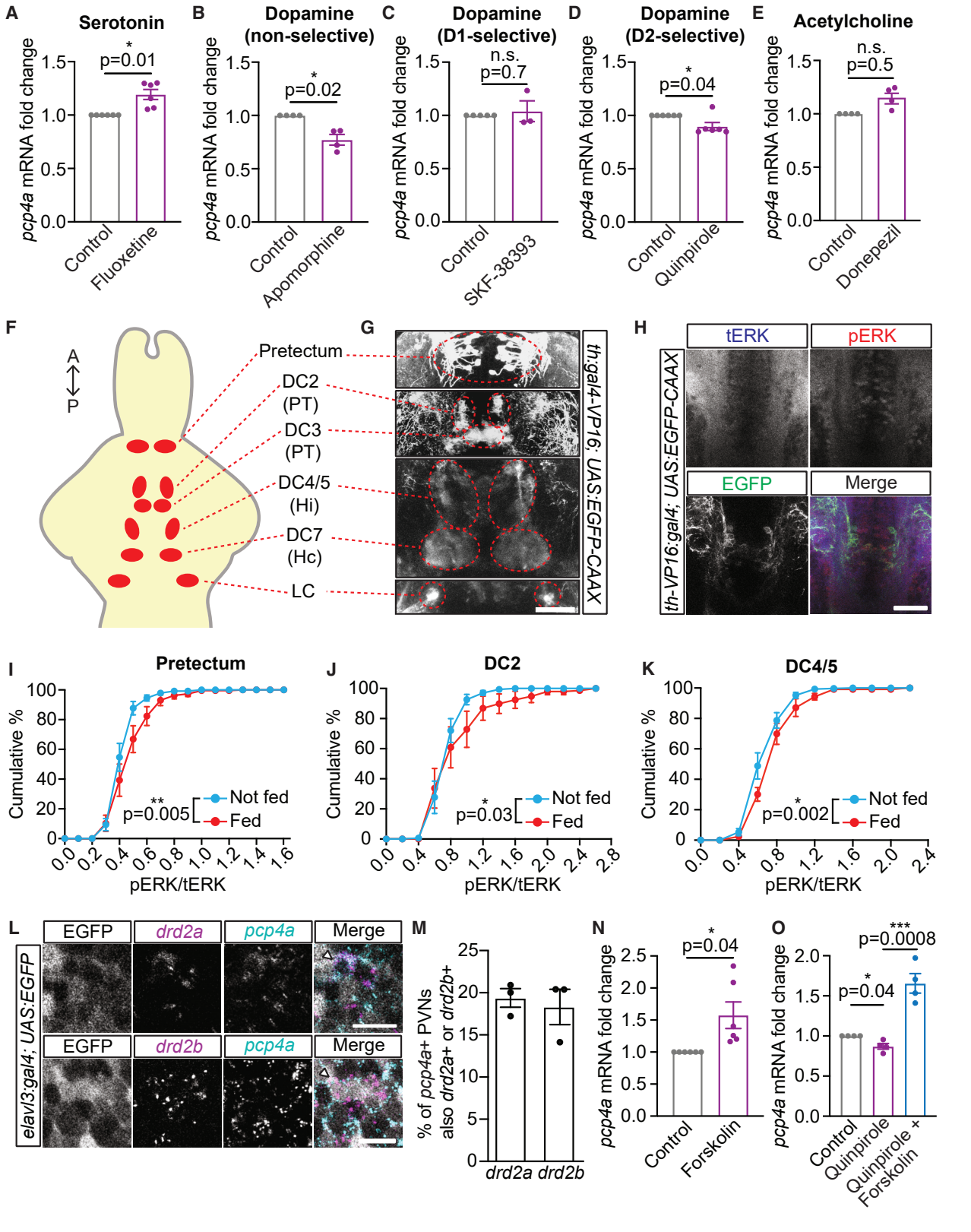

(legend on next page)

Please cite this article in press as: Zaupa et al., The Calmodulin-interacting peptide Pcp4a regulates feeding state-dependent behavioral choice in zebrafish, Neuron (2024), https://doi.org/10.1016/j.neuron.2024.01.001

the effect of food deprivation,[30] we tested whether increasing serotonergic transmission with the selective serotonin reuptake inhibitor fluoxetine in fed larvae could lead to changes of *pcp4a*'s expression. After treating 7 dpf fed fish for 4 h with fluoxetine, we performed RT-qPCR with samples obtained from their dissected brains. In accord with our hypothesis, we found that *pcp4a* was upregulated by fluoxetine (Figure 4A). However, the increase of *pcp4a*'s expression was relatively small. We therefore wondered if other neurotransmitters could also contribute to regulate transcription of *pcp4a*. We decided to interfere with dopaminergic transmission because it was also shown to modulate decision-making.[46,47] Since several studies showed that in mammals food intake induces release of dopamine,[48] and considering the fact that we observed reduced expression of *pcp4a* in fed fish, we tested whether activating dopaminergic transmission in food-deprived larvae could reduce expression of *pcp4a*. Interestingly, treating 7 dpf food-deprived WT larvae with the non-subtype-selective dopamine receptor agonist apomorphine decreased expression of *pcp4a* (Figure 4B). Dopamine receptors are divided into two groups: D1-like (D1 and D5 subtypes) and D2-like (D2, D3, and D4 subtypes).[49] To identify the type of receptor mediating the effect of dopamine on *pcp4a*'s expression, we treated 7 dpf food-deprived WT larvae with either the D1-like-selective agonist SKF-38393 or the D2-like-selective agonist quinpirole. Quinpirole, but not SKF-38393, was able to reduce expression of *pcp4a* (Figures 4C and 4D), indicating that D2-like, but not D1-like, receptors activate a signaling cascade leading to repression of *pcp4a*'s expression. We also tested whether cholinergic transmission could regulate expression of *pcp4a*. However, we found that enhancing cholinergic transmission with the cholinesterase inhibitor donepezil in food-deprived WT larvae did not induce changes of *pcp4a*'s mRNA level (Figure 4E).

Since we observed that dopaminergic signaling is able to inhibit transcription of *pcp4a*—the same effect induced by feeding—we next tested whether food intake is capable of activating dopaminergic neurons in the zebrafish brain, which are subdivided in several clusters[50,51] (Figures 4F and 4G). To this end, we used intensity of immunofluorescence staining of phosphorylated extracellular signal-regulated kinase (pERK), normalized by intensity of immunofluorescence staining of total (phosphorylated and not) ERK (tERK), as a proxy of neuronal activity.[52] We found that in 7 dpf *th:gal4-VP16; UAS:EGFP-CAAX* fish (Figures 4G and 4H), in which dopaminergic and noradrenergic neurons are labeled,[53] dopaminergic neurons in the pretectum, DC2, and DC4/5 groups were activated by food intake (Figures 4I–4K), while activity of neurons in the DC3 and DC7 groups was not altered (Figures S5A and S5B). Furthermore, activity of noradrenergic neurons in the locus coeruleus was also not changed by feeding (Figure S5C). We were not able to measure activity of the DC1 and DC6 dopaminergic groups because they were not consistently labeled in the *th:gal4-VP16; UAS:EGFP-CAAX* line.

Several dopaminergic neurons, including the ones in the pretectum and in the DC1, DC2, DC4, and DC5 clusters, project axons to the tectum.[51] It is therefore possible that dopaminergic transmission via D2-like receptors could directly control expression of *pcp4a* in tectal PVNs. In support of this hypothesis, we found that a fraction of *pcp4a*+ PVNs express the two zebrafish D2-receptor-coding paralogous genes *drd2a* and *drd2b* (Figures 4L and 4M). We next investigated how dopaminergic transmission could alter expression of *pcp4a*. Activation of D2-like receptors leads to inhibition of cyclic AMP (cAMP) production by the enzyme adenylate cyclase, and subsequent repression of target genes expression via the protein kinase A (PKA)-cAMP response element-binding protein (CREB) pathway.[49] We therefore reasoned that if *pcp4a*'s expression is repressed by D2 receptors through inhibition of this pathway, increasing amounts of intracellular cAMP should induce expression of *pcp4a*. Indeed, we found that treating WT zebrafish larvae for 1 h with the adenylate cyclase activator forskolin increased *pcp4a*'s expression (Figure 4N). Moreover, as further confirmation that adenylate cyclase acts downstream of D2-type receptors to regulate expression of *pcp4a*, we observed that forskolin could rescue quinpirole-induced repression of the gene's expression (Figure 4O).

These data suggest that food intake in zebrafish activates a subset of dopaminergic neurons, which represses expression of *pcp4a* through D2-like receptor-mediated inhibition of cAMP production. Concurrently, feeding also reduces serotonergic transmission,[30] inhibiting its effect on induction of *pcp4a*'s transcription.

Figure 4. Serotonergic and dopaminergic transmission regulates expression of *pcp4a*

(A–E) Graphs showing average *pcp4a* mRNA fold change in the brains of wild-type fish fed and treated with fluoxetine (A), or food deprived and treated with apomorphine (B), SKF-38393 (C), quinpirole (D), or donepezil (E). mRNA amounts were normalized to control clutchmates. n = 6 in (A) and (D), n = 4 in (B) and (E), n = 3 in (C). n indicates the number of biological replicas (pool of ten brains per replica).

(F and G) Scheme (F) and confocal images of a 7 dpf *th:gal4-VP16; UAS:EGFP-CAAX* larva (G), showing localization of dopaminergic and noradrenergic (locus coeruleus) neuronal clusters. Scale bars in (G), 50 μm.

(H) Confocal images of a 7 dpf *th:gal4-VP16; UAS:EGFP-CAAX* larva immunostained with antibodies against GFP, pERK, and tERK. Scale bars, 50 μm.

(I–K) Graphs depicting cumulative percentages of pERK/tERK values in dopaminergic neurons in fed or food-deprived 7 dpf *th:gal4-VP16; UAS:EGFP-CAAX* larvae. n = 9 larvae (I and J) or n = 10 (K), for each condition.

(L) Confocal images of 7 dpf *elavl3:gal4; UAS:EGFP* larvae, showing localization of *pcp4a*, *drd2a*, and *drd2b* mRNA in GFP-labeled tectal PVNs. Scale bars, 10 μm.

(M) Bar graph depicting average percentages of *pcp4a*+ tectal PVNs expressing either *drd2a* or *drd2b*. n = 3 larvae.

(N and O) Bar graphs showing average *pcp4a* mRNA fold change in 5 dpf wild-type fish treated with forskolin (N), or in 7 dpf wild-type larvae treated first with quinpirole for 2 h and then with quinpirole and forskolin for 1 h. mRNA amounts were normalized to control clutchmates. n = 6 (N) or n = 4 (O) biological replicas (pool of ten larvae per replica) per group. * $p < 0.05$, ** $p < 0.01$, and *** $p < 0.001$; n.s., not significant; one-sample t test (A–E, N, and O [control vs. quinpirole]), two-tailed t test (O, quinpirole vs. quinpirole + forskolin), or two-way ANOVA (I–K). Data in the graphs are shown as mean ± standard error of the mean.

See also Figure S5.

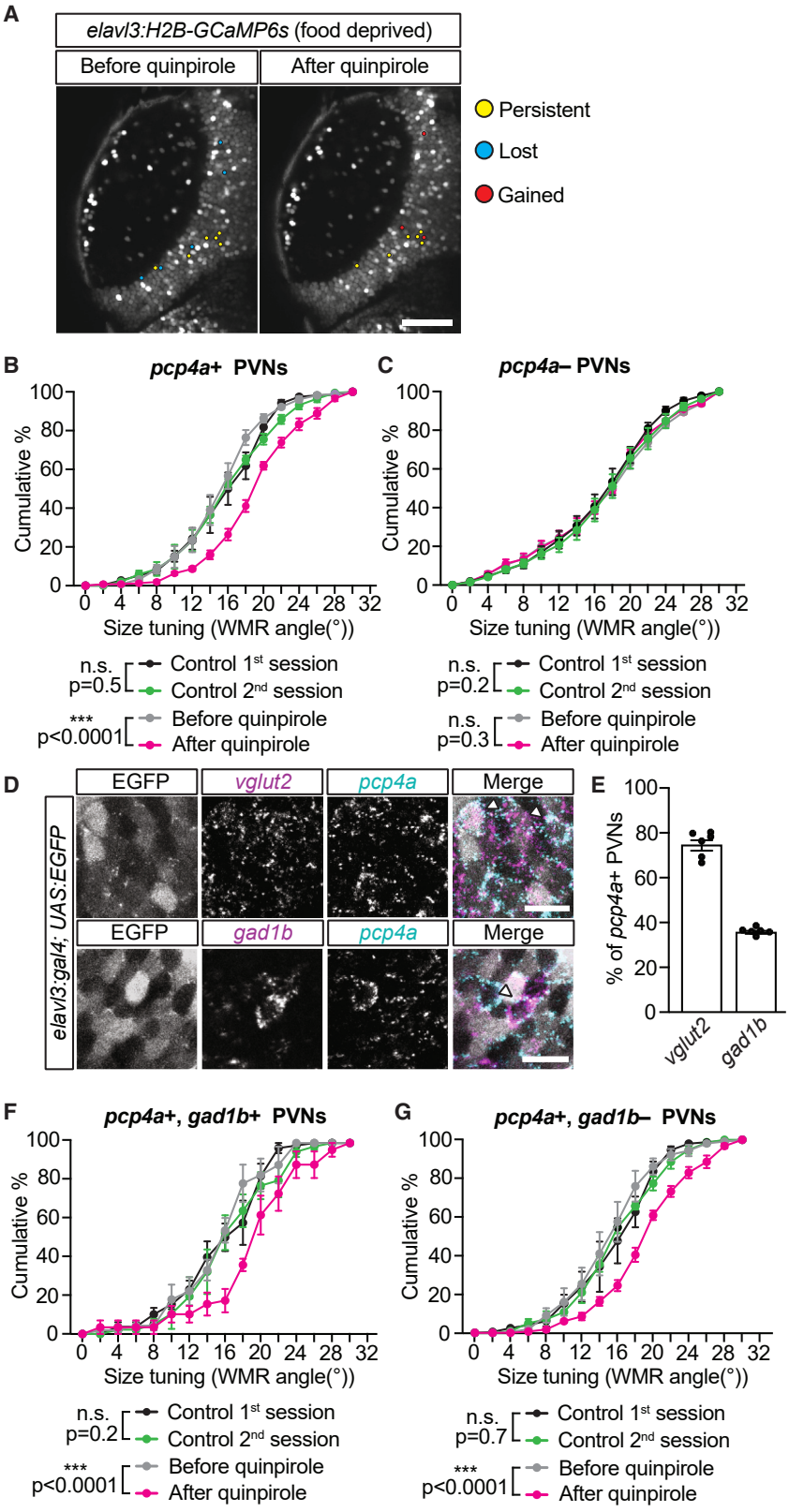

Figure 5. Activation of dopamine D2-like receptors modulates visual size representation in the tectum

(A) Images showing part of the tectum of a food-deprived 7 dpf *elavl3:H2B-GCaMP6s* larva before and after treatment with quinpirole. Scale bars, 50 μm.

(B and C) Graphs depicting cumulative percentages of WMR angles of *pcp4a*+ (B) or *pcp4a*− (C) PVNs in unfed 7 dpf *elavl3:H2B-GCaMP6s* larvae before and after 3-h treatment with quinpirole or in control unfed 7 dpf *elavl3:H2B-GCaMP6s* fish not treated with quinpirole but kept in agarose for the same duration of the drug treatment. n = 5 fish per group.

(D) Confocal images showing localization of *pcp4a*, *vglut2*, and *gad1b* mRNA in tectal PVNs in 7 dpf *elavl3:gal4, UAS:EGFP* larvae. Scale bars, 10 μm.

(E) Bar graph showing percentages of glutamatergic (*vglut2*+) or GABAergic (*gad1b*+) *pcp4a*+ PVNs. n = 6 larvae per group.

(F and G) Graphs showing cumulative percentages of WMR angles of *pcp4a*+ and *gad1b*+ (F) or *pcp4a*+ and *gad1b*− (G) PVNs in unfed 7 dpf *elavl3:H2B-GCaMP6s* larvae before and after 3-h treatment with quinpirole or in control unfed 7 dpf *elavl3:H2B-GCaMP6s* fish not treated with quinpirole, imaged in two consecutive sessions 3 h apart. Data in these graphs are subsets of the data shown in (B). n = 4 fish per group. ***p < 0.001; n.s., not significant; two-way ANOVA. Data are shown as mean ± standard error of the mean.

See also Figure S6.

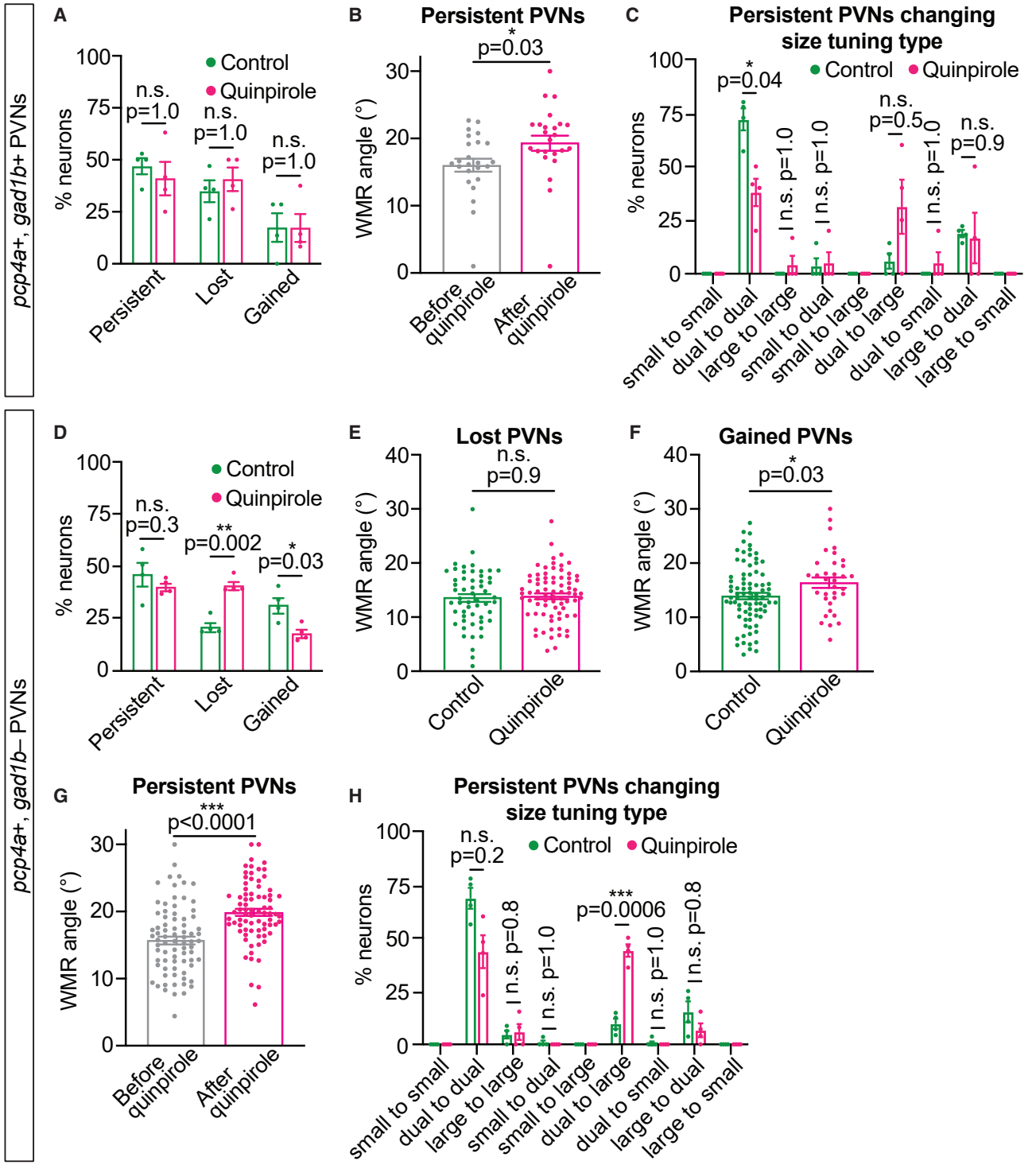

Figure 6. Dopamine D2-like receptor signaling modifies visual size tuning of *gad1b*+ and *gad1b*– *pcp4a*+ PVNs

(A) Bar graph depicting percentages of *pcp4a*+/*gad1b*+ PVNs, imaged in two sessions 3 h apart, classified as persistent, lost, and gained in quinpirole-treated and untreated (control) 7 dpf *elavl3:H2B-GCaMP6s* larvae. n = 4 fish per group.

(B) Graph showing tuning size (WMR angle) of persistent *pcp4a*+/*gad1b*+ PVNs before and after quinpirole treatment. n = 24 neurons from 4 larvae.

(C) Graph displaying percentages of persistent *pcp4a*+/*gad1b*+ PVNs changing response type in the two imaging sessions. Small, neurons responding to circles $\leq 5°$; large, neurons responding to circles $\geq 10°$; dual, neurons responding to both types of stimuli. n = 4 larvae per group.

(D) Graph showing percentages of persistent, lost, and gained *pcp4a*+/*gad1b*− PVNs in quinpirole-treated and untreated (control) larvae. n = 4 fish per group.

(legend continued on next page)

Dopaminergic transmission modifies size tuning of tectal *pcp4a*+ PVNs

We previously showed that serotonergic transmission, which is enhanced by food deprivation, modifies population responses of tectal PVNs by inducing activation of neurons responsive to small-sized visual stimuli.[30] We therefore asked whether activation of dopamine D2-like receptors could also change visual size representation in the tectum. We performed an experiment in which we first recorded responses of tectal PVNs to visual stimuli of different sizes, using calcium imaging in 7 dpf food-deprived *elavl3:H2B-GCaMP6s* fish. We then treated the larvae, still embedded in agarose, with the dopamine D2-like receptor agonist quinpirole for 3 h. Afterward, we performed calcium imaging again to monitor responses to visual stimuli of the PVNs imaged during the first session. Finally, we identified *pcp4a*+ neurons with post-mortem *in situ* HCR and alignment of the *in vivo* and post-mortem image stacks. With this strategy, we were able to directly compare size tuning of individual PVNs before and after treatment with quinpirole (Figures 5A, S6A, and S6B). We identified three major classes of neurons based on their responses in the two imaging sessions: persistent (responding to visual stimuli of any size in both sessions), lost (responding only in the first session to stimuli of any size), and gained (responding only in the second session to stimuli of any size). Interestingly, we found that quinpirole shifted the response profile of *pcp4a*+ PVNs toward large sizes of the visual stimuli (Figure 5B), similar to the change caused by the *pcp4a*^{md78} mutation (Figure 3F) or by food intake (Figure 3D). In contrast, treatment with quinpirole did not have a major impact on responses to visual stimuli in *pcp4a*− PVNs (Figure 5C). Moreover, we did not detect changes of size tuning between the two imaging sessions in PVNs of fish not treated with quinpirole (Figure 5B). Interestingly, we found that treating unfed *pcp4a*$^{md78/md78}$*; elavl3:H2B-GCaMP6s* larvae with quinpirole did not alter responses to visual stimuli in *pcp4a*+ PVNs (Figure S6C). These data suggest that activation of dopamine D2-like receptors alters size tuning of *pcp4a*+ tectal PVNs, mainly through the downstream action of Pcp4a.

To better understand how D2-like receptor signaling modifies size representation in the tectum, we identified the neurotransmitter phenotype of *pcp4a*+ PVNs. Using *in situ* HCR to detect mRNAs coding for *pcp4a*, *vglut2* (a glutamatergic marker), and *gad1b* (a GABAergic marker), we found that the majority (75.1% ± 2.3%) of *pcp4a*+ PVNs in the tectum are glutamatergic, while a smaller population (36.2% ± 0.6%) is GABAergic (Figures 5D and 5E). We next investigated if D2-like receptor activation modulates representation of visual stimulus size in both populations of *pcp4a*+ neurons. To this end, we performed *in situ* HCR to detect *gad1b* mRNA in the larvae previously used for the calcium imaging experiment in which responses of PVNs were recorded before and after treatment with quinpirole (Figures 5B and 5C). In this way, we were able to classify the PVNs as *gad1b*+ and *gad1b*− (most likely glutamatergic, as the majority of *pcp4a*+ PVNs are *vglut2*+). Interestingly, we found that quinpirole shifted the population response of both *gad1b*+ and *gad1b*− toward large visual stimulus size (Figures 5F and 5G).

Next, we took advantage of the fact that we could monitor activity of individual neurons before and after addition of quinpirole to better understand how changes of response profile of single neurons lead to the population shift of visual size representation. In *pcp4a*+/*gad1b*+ PVNs, we did not observe a net change of number of neurons of the persistent, lost, and gained types after quinpirole treatment, compared with untreated controls (Figure 6A). However, we found that quinpirole altered the size tuning of the persistent neurons by making them more responsive to large stimuli than small ones (Figure 6B). This change was largely due to dual-responding neurons, which were activated by both small ($\leq 5°$) and large ($\geq 10°$) circles, becoming responsive only to large stimuli (Figure 6C). We did not detect alterations of size tuning in control untreated fish during the two imaging sessions (Figure S6D). In the *pcp4a*+/*gad1b*− subpopulation, there was a net loss of visual-responsive neurons due to increased numbers of lost PVNs and decreased numbers of gained ones in the tecta of quinpirole-treated fish, compared with untreated controls (Figure 6D). While size tuning of lost PVNs did not differ between quinpirole-treated and untreated fish (Figure 6E), gained neurons were, on average, tuned to larger visual stimuli (Figure 6F). In addition, we also observed that tuning of the persistent type of neurons was also shifted toward larger stimuli by quinpirole (Figure 6G), but not in control untreated larvae (Figure S6E). Similar to what we observed in the *pcp4a*+/*gad1b*+ PVNs, also in *pcp4a*+/*gad1b*− neurons this shift was largely due to suppression of responses to small stimuli in dually tuned neurons, which became activated only by large visual stimuli (Figure 6H).

Taken together, these results suggest that activation of dopamine D2-like receptors alters visual stimulus size representation in both glutamatergic and GABAergic *pcp4a*+ neurons, largely by suppressing activation of dually tuned PVNs by small visual stimuli.

DISCUSSION

While molecular events regulating some cognitive functions such as learning and memory are known in great detail,[22] little is known about biochemical pathways responsible for behavioral choice. Studies in invertebrates have identified several

(E and F) Bar graphs depicting size tuning (WMR angle) of lost (E) or gained (F) *pcp4a*+/*gad1b*− PVNs in fish treated with quinpirole and untreated controls. $n_{Lost\text{-}Control}$ = 55 neurons from 4 larvae, $n_{Lost\text{-}Quinpirole}$ = 76 neurons from 4 larvae, $n_{Gained\text{-}Control}$ = 82 neurons from 4 larvae, $n_{Gained\text{-}Quinpirole}$ = 34 neurons from 4 larvae. *p = 0.03; n.s., not significant; nested two-way ANOVA.

(G) Graph showing WMR angles of persistent *pcp4a*+/*gad1b*− PVNs before and after quinpirole treatment. n = 77 neurons from 4 larvae.

(H) Graph displaying percentages of persistent *pcp4a*+/*gad1b*− PVNs changing response type in the two imaging sessions. n = 4 larvae per group. *p < 0.05, **p < 0.01, and ***p < 0.001; n.s., not significant; t test with Bonferroni-Holm correction (A, C, D, and H), paired t test (B and G), or nested two-way ANOVA (E and F). Data are shown as mean ± standard error of the mean.

See also Figure S6.

Please cite this article in press as: Zaupa et al., The Calmodulin-interacting peptide Pcp4a regulates feeding state-dependent behavioral choice in zebrafish, Neuron (2024), https://doi.org/10.1016/j.neuron.2024.01.001

neurotransmitters and neuropeptides involved in decision-making.[16,17] A number of these neurotransmitters were shown to play crucial roles also in decision-making in rodents,[54] and possibly humans.[9,21,47,54] These findings point to the existence of fundamental, evolutionarily conserved, mechanisms regulating behavioral choice. However, the molecular events downstream of the neurotransmitter receptors have remained largely elusive.

Recently, robust behavioral assays have been used to quantitatively analyze behavioral choice in zebrafish. With these assays, neuronal circuits underlying evidence accumulation leading to action selection,[55,56] initiation of alternative escape strategies in response to acoustic/vibrational stimuli,[57,58] and choice of approach or avoidance of visual stimuli[29,30] have been revealed.

Now, our work identified the Calmodulin-interacting peptide Pcp4a as a key regulator of behavioral choice in zebrafish. We found that abundance of Pcp4a in the brain is regulated by feeding state. Food intake represses expression of *pcp4a* in the brain, and mutating *pcp4a* induces food-deprived fish to behave like fed ones by making them take less risks in an approach/avoidance decision assay. This finding pinpoints the identity of an intracellular regulator of behavioral selection in a vertebrate and may pave the way to a better understanding of the molecular basis of action selection also in mammals.

Pcp4a is expressed in a subpopulation of neurons in the tectum[39] (Figures 1C, 3E, and S1A), a brain region homologous to the mammalian superior colliculus, centrally involved in regulating prey capture and avoidance of threats.[32] Tectal PVNs display several types of visual size selectivity, with some of them tuned specifically to either small or large stimuli, whereas others respond to a wide range of stimulus sizes.[59–61] Stimulus size representation in the tectum is an important process regulating sensory-motor transformations, leading to approach of prey and avoidance of predators.[28,42] We previously showed that food intake reduces responses of tectal PVNs to small visual stimuli. Here, we found that mutating *pcp4a* has a similar effect. How could changing size representation in the tectum modulate foraging-related decisions? Filtering of sensory information at early stages of sensory processing could represent an efficient way to bias action selection, for example, by enhancing responsiveness to stimuli promoting actions best suited to deal with current environmental and internal state conditions, while suppressing other stimuli that drive competing behaviors.[16] In accord with a previous study,[39] we found that *pcp4a* is expressed also by additional discrete populations of neurons in other regions of the central nervous system, including the retina, pretectum, medulla oblongata, and spinal cord (Figure S1). It may be that expression of pcp4a in these regions could also be modulated by food intake and that Pcp4a in subsets of neurons outside the tectum could also contribute to the effect of feeding on behavioral choice. Novel molecular tools allowing mutation of *pcp4a* in subpopulations of neurons will be required to test this hypothesis.

We found that enhancing serotonergic transmission with fluoxetine increases expression of *pcp4a*. This action of serotonin is in agreement with our previous results showing that food deprivation in zebrafish activates serotonergic neurons in the raphe nucleus and that enhancing serotonergic transmission increases responses to small visual stimuli in tectal PVNs.[30] However, the effect of fluoxetine on *pcp4a*'s expression was relatively subtle, suggesting that more than one neurotransmitter system contribute to regulate transcription of *pcp4a*. Indeed, we showed that activating dopamine D2-like receptors represses transcription of *pcp4a* and reduces responses of tectal *pcp4a*+ PVNs to small visual stimuli, a phenotype that is also present in homozygous *pcp4a* mutants.

Accordingly, we found that food intake activates several groups of dopaminergic neurons in the zebrafish brain. These results agree with previous findings in rodents and humans showing that food ingestion induces activation of the dopaminergic system,[48,62] and they further expand our understanding of the role of dopamine in decision-making. Our data showed that two D2 receptors, *drd2a* and *drd2b*, are expressed by tectal *pcp4a*+ PVNs, suggesting that dopamine could act directly on these neurons to regulate expression of *pcp4a*. In support of this hypothesis, it was shown that axons belonging to several of the dopaminergic neurons found to be activated by food intake in our study, including the ones in the pretectum and in the DC2, DC4, and DC5 groups, are present in the tectum.[51]

Binding of dopamine to D2-like receptors represses production of cAMP by the enzyme adenylate cyclase,[49] and we showed here that enhancing adenylate cyclase activity increases transcription of *pcp4a*. cAMP is well known to regulate transcription of genes via PKA-dependent phosphorylation of the transcription factor CREB.[63] Expression of *pcp4a* is therefore negatively controlled by dopaminergic transmission likely via inhibition of this signaling pathway.

Pcp4a acts most likely in a cell-autonomous way in regulating responses of PVNs to visual stimuli, since we found that the effect of mutating *pcp4a* is mostly limited to neurons expressing the gene. In support of this hypothesis, we found that activity of SINs, which were shown to be involved in regulating size filtering of visual information,[42,43] and responses to visual stimuli in RGC axons were not altered in *pcp4a* mutants. However, we found that a very small population of RGCs expresses *pcp4a*. Considering the low number of these cells, it is possible that we could not detect Pcp4a-mediated modulation of their activity when we analyzed visual response properties of the whole population of RGCs, and we cannot completely rule out their potential involvement in modulating size tuning of tectal PVNs.

In *pcp4a* mutants, responses of *pcp4a*+ PVNs to small visual stimuli are reduced, suggesting that Pcp4a selectively enhances this type of responses in the tectum. There are two main ways by which Pcp4a could induce this size-specific modulation: by promoting activation of neurons responding only to small stimuli or by selectively enhancing responses to small stimuli in dually tuned neurons. Interestingly, we found that the major effect of activating dopaminergic D2-like receptors, which represses expression of *pcp4a*, was to suppress responses to small visual stimuli in dually tuned *pcp4a*+ PVNs, which are the most abundant population of *pcp4a*+ PVNs in the tectum (Figures 6C and 6H). PVNs that are activated by both small and large visual stimuli were previously observed.[29,59–61] However, their role in sensory-motor transformations, and particularly in action selection, is unknown. Our findings uncovered a potentially important role of this class of tectal neurons in regulating decision-making. We

observed that feeding state is capable of altering visual responses in both *pcp4a*+ and *pcp4a*− neurons, suggesting that multiple circuit mechanisms for modulating foraging behavior may exist in the tectum, likely involving diverse types of neurons and multiple modulatory systems, including the dopaminergic and serotonergic ones.[30]

How could modification of size tuning in dually tuned *pcp4a*+ PVNs induce changes of approach/avoidance behavior? It is possible that they could integrate information about both potential preys and predators and act at a critical circuit interface of sensory and motor networks, where they could be optimal targets of neuromodulatory circuits activated by feeding state for biasing motor outputs toward approach or avoidance, depending on the physiological state of the animal. Such a role at a critical circuit node could also explain their relative low number in the tectum (circa 3% of tectal PVNs are both *pcp4a*+ and *drd2a/b*+, according to our estimation). The SINs, another small population of tectal neurons, regulate filtering of visual size information entering the tectum.[42,43] The *pcp4a*+ PVNs identified by us may act in a similar fashion at the output stage. The fact that activation of D2-like receptors affects size tuning of both GABAergic and non-GABAergic dually tuned *pcp4a*+ PVNs suggests that multiple subtypes of neurons may be involved.

It is possible that Pcp4a regulates postsynaptic activity in these neurons in a synapse-specific manner. This specificity could be achieved, for example, by localizing Pcp4a or dopamine receptors, or both, to synapses receiving inputs conveying information about small stimuli. Alternatively, the activation mode of different synapses could lead to different dynamics of Pcp4a-mediated suppression of CaMKII activity, which we have shown to be important for mediating the action of Pcp4a on modulation of size tuning, in line with a previous *in vitro* study showing that inhibition of CaMKII by mammalian PCP4 depends on the type of intracellular calcium mobilization.[34] Our finding that Pcp4a modulates size tuning of PVNs via CaMKII indicates that its molecular mode of action is conserved across vertebrates, and it also points to a previously unknown role of this molecular interaction in modulating sensory-motor transformations.

STAR★METHODS

Detailed methods are provided in the online version of this paper and include the following:

SUPPLEMENTAL INFORMATION

Supplemental information can be found online at https://doi.org/10.1016/j.neuron.2024.01.001.

ACKNOWLEDGMENTS

We would like to thank Anne Banerjee and the staff of the Zebrafish Facility and the Advanced Light Microscopy Technology Platform at the Max Delbrück Center for Molecular Medicine for technical support. We are also thankful to Marco dal Maschio for advice on analysis of calcium imaging data. This work was supported by the Helmholtz Association of German Research Centers, the Max Planck Society, and by grants from the German Research Foundation (Deutsche Forschungsgemeinschaft, project ID: FI 2339/1-1, and SFB 870 – Assembly and Function of Neural Circuits, TP16).

AUTHOR CONTRIBUTIONS

A.F. conceived and designed all experiments, some of which were started in H.B.'s laboratory and were continued in his own laboratory; provided supervision; administered the project; and performed data analyses. S.S. and H.B. provided supervision. M.Z. and N.N. designed and performed experiments and analyzed data. A.S. analyzed data. A.F. and M.Z. wrote the manuscript, with contributions by H.B. All authors commented on the manuscript.

DECLARATION OF INTERESTS

The authors declare no competing interests.

Received: March 1, 2023
Revised: October 6, 2023
Accepted: January 2, 2024
Published: January 30, 2024

REFERENCES

1. Rangel, A., Camerer, C., and Montague, P.R. (2008). A framework for studying the neurobiology of value-based decision making. Nat. Rev. Neurosci. *9*, 545–556.
2. Palmer, C.R., and Kristan, W.B. (2011). Contextual modulation of behavioral choice. Curr. Opin. Neurobiol. *21*, 520–526.
3. Phelps, E.A., Lempert, K.M., and Sokol-Hessner, P. (2014). Emotion and Decision Making: Multiple Modulatory Neural Circuits. Annu. Rev. Neurosci. *37*, 263–287.
4. Kennedy, A., Asahina, K., Hoopfer, E., Inagaki, H., Jung, Y., Lee, H., Remedios, R., and Anderson, D.J. (2014). Internal States and Behavioral Decision-Making: Toward an Integration of Emotion and Cognition. Cold Spring Harb. Symp. Quant. Biol. *79*, 199–210.
5. Hirayama, K., and Gillette, R. (2012). A Neuronal Network Switch for Approach/Avoidance Toggled by Appetitive State. Curr. Biol. *22*, 118–123.
6. Bräcker, L.B., Siju, K.P., Varela, N., Aso, Y., Zhang, M., Hein, I., Vasconcelos, M.L., and Grunwald Kadow, I.C. (2013). Essential Role of the Mushroom Body in Context-Dependent CO_2 Avoidance in Drosophila. Curr. Biol. *23*, 1228–1234.
7. Inagaki, H.K., Panse, K.M., and Anderson, D.J. (2014). Independent, Reciprocal Neuromodulatory Control of Sweet and Bitter Taste Sensitivity during Starvation in Drosophila. Neuron *84*, 806–820.
8. Smith, N.K., and Grueter, B.A. (2022). Hunger-driven adaptive prioritization of behavior. FEBS Journal *289*, 922–936.

9. Liu, L., Artigas, S.O., Ulrich, A., Tardu, J., Mohr, P.N.C., Wilms, B., Koletzko, B., Schmid, S.M., and Park, S.Q. (2021). Eating to dare - Nutrition impacts human risky decision and related brain function. NeuroImage *233*, 117951.

10. Padilla, S.L., Qiu, J., Soden, M.E., Sanz, E., Nestor, C.C., Barker, F.D., Quintana, A., Zweifel, L.S., Rønnekleiv, O.K., Kelly, M.J., et al. (2016). Agouti-related peptide neural circuits mediate adaptive behaviors in the starved state. Nat. Neurosci. *19*, 734–741.

11. Burgess, C.R., Ramesh, R.N., Sugden, A.U., Levandowski, K.M., Minnig, M.A., Fenselau, H., Lowell, B.B., and Andermann, M.L. (2016). Hunger-Dependent Enhancement of Food Cue Responses in Mouse Postrhinal Cortex and Lateral Amygdala. Neuron *91*, 1154–1169.

12. Critchley, H.D., and Rolls, E.T. (1996). Hunger and satiety modify the responses of olfactory and visual neurons in the primate orbitofrontal cortex. J. Neurophysiol. *75*, 1673–1686.

13. Burgess, C.R., Livneh, Y., Ramesh, R.N., and Andermann, M.L. (2018). Gating of visual processing by physiological need. Curr. Opin. Neurobiol. *49*, 16–23.

14. LaBar, K.S., Gitelman, D.R., Parrish, T.B., Kim, Y.H., Nobre, A.C., and Mesulam, M.M. (2001). Hunger selectively modulates corticolimbic activation to food stimuli in humans. Behav. Neurosci. *115*, 493–500.

15. Cornier, M.A., Von Kaenel, S.S., Bessesen, D.H., and Tregellas, J.R. (2007). Effects of overfeeding on the neuronal response to visual food cues. Am. J. Clin. Nutr. *86*, 965–971.

16. Gaudry, Q., and Kristan, W.B. (2009). Behavioral choice by presynaptic inhibition of tactile sensory terminals. Nat. Neurosci. *12*, 1450–1457.

17. Yapici, N., Zimmer, M., and Domingos, A.I. (2014). Cellular and molecular basis of decision-making. EMBO Rep. *15*, 1023–1035.

18. Heekeren, H.R., Marrett, S., and Ungerleider, L.G. (2008). The neural systems that mediate human perceptual decision making. Nat. Rev. Neurosci. *9*, 467–479.

19. Kristan, W.B. (2008). Neuronal Decision-Making Circuits. Curr. Biol. *18*, R928–R932.

20. Cheong, H.S., Siwanowicz, I., and Card, G.M. (2020). Multi-regional circuits underlying visually guided decision-making in Drosophila. Curr. Opin. Neurobiol. *65*, 77–87.

21. Takahashi, H. (2012). Monoamines and assessment of risks. Curr. Opin. Neurobiol. *22*, 1062–1067.

22. Ortega-de San Luis, C., and Ryan, T.J. (2022). Understanding the physical basis of memory: Molecular mechanisms of the engram. J. Biol. Chem. *298*, 101866.

23. Corradi, L., and Filosa, A. (2021). Neuromodulation and Behavioral Flexibility in Larval Zebrafish: From Neurotransmitters to Circuits. Front. Mol. Neurosci. *14*, 718951.

24. Semmelhack, J.L., Donovan, J.C., Thiele, T.R., Kuehn, E., Laurell, E., and Baier, H. (2014). A dedicated visual pathway for prey detection in larval zebrafish. eLife *3*, e04878.

25. Budick, S.A., and O'Malley, D.M. (2000). Locomotor repertoire of the larval zebrafish: swimming, turning and prey capture. J. Exp. Biol. *203*, 2565–2579.

26. Bianco, I.H., Kampff, A.R., and Engert, F. (2011). Prey Capture Behavior Evoked by Simple Visual Stimuli in Larval Zebrafish. Front. Syst. Neurosci. *5*, 101.

27. Temizer, I., Donovan, J.C., Baier, H., and Semmelhack, J.L. (2015). A Visual Pathway for Looming-Evoked Escape in Larval Zebrafish. Curr. Biol. *25*, 1823–1834.

28. Dunn, T.W., Gebhardt, C., Naumann, E.A., Riegler, C., Ahrens, M.B., Engert, F., and Del Bene, F. (2016). Neural Circuits Underlying Visually Evoked Escapes in Larval Zebrafish. Neuron *89*, 613–628.

29. Barker, A.J., and Baier, H. (2015). Sensorimotor Decision Making in the Zebrafish Tectum. Curr. Biol. *25*, 2804–2814.

30. Filosa, A., Barker, A.J., Dal Maschio, M., and Baier, H. (2016). Feeding State Modulates Behavioral Choice and Processing of Prey Stimuli in the Zebrafish Tectum. Neuron *90*, 596–608.

31. Roeser, T., and Baier, H. (2003). Visuomotor Behaviors in Larval Zebrafish after GFP-Guided Laser Ablation of the Optic Tectum. J. Neurosci. *23*, 3726–3734.

32. Isa, T., Marquez-Legorreta, E., Grillner, S., and Scott, E.K. (2021). The tectum/superior colliculus as the vertebrate solution for spatial sensory integration and action. Curr. Biol. *31*, R741–R762.

33. Bollmann, J.H. (2019). The Zebrafish Visual System: From Circuits to Behavior. Annu. Rev. Vis. Sci. *5*, 269–293.

34. Johanson, R.A., Sarau, H.M., Foley, J.J., and Slemmon, J.R. (2000). Calmodulin-Binding Peptide PEP-19 Modulates Activation of Calmodulin Kinase II *In Situ*. J. Neurosci. *20*, 2860–2866.

35. Slemmon, J.R., Feng, B., and Erhardt, J.A. (2000). Small Proteins that Modulate Calmodulin-Dependent Signal Transduction: Effects of PEP-19, neuromodulin, and neurogranin on enzyme activation and cellular homeostasis. Mol. Neurobiol. *22*, 99–113.

36. Burgoyne, R.D. (2007). Neuronal calcium sensor proteins: generating diversity in neuronal Ca2+ signalling. Nat. Rev. Neurosci. *8*, 182–193.

37. Xia, Z., and Storm, D.R. (2005). The role of calmodulin as a signal integrator for synaptic plasticity. Nat. Rev. Neurosci. *6*, 267–276.

38. Wei, P., Blundon, J.A., Rong, Y., Zakharenko, S.S., and Morgan, J.I. (2011). Impaired Locomotor Learning and Altered Cerebellar Synaptic Plasticity in *pep-19*/*pcp4*-Null Mice. Mol. Cell. Biol. *31*, 2838–2844.

39. Mione, M., Lele, Z., Kwong, C.T., Concha, M.L., and Clarke, J.D. (2006). Expression of pcp4a in subpopulations of CNS neurons in zebrafish. J. Comp. Neurol. *495*, 769–787.

40. Freeman, J., Vladimirov, N., Kawashima, T., Mu, Y., Sofroniew, N.J., Bennett, D.V., Rosen, J., Yang, C.T., Looger, L.L., and Ahrens, M.B. (2014). Mapping brain activity at scale with cluster computing. Nat. Methods *11*, 941–950.

41. Choi, H.M.T., Schwarzkopf, M., Fornace, M.E., Acharya, A., Artavanis, G., Stegmaier, J., Cunha, A., and Pierce, N.A. (2018). Third-generation *in situ* hybridization chain reaction: multiplexed, quantitative, sensitive, versatile, robust. Development *145*, dev165753.

42. Del Bene, F., Wyart, C., Robles, E., Tran, A., Looger, L., Scott, E.K., Isacoff, E.Y., and Baier, H. (2010). Filtering of Visual Information in the Tectum by an Identified Neural Circuit. Science *330*, 669–673.

43. Barker, A.J., and Baier, H. (2013). SINs and SOMs: neural microcircuits for size tuning in the zebrafish and mouse visual pathway. Front. Neural Circuits *7*, 89.

44. Yasuda, R., Hayashi, Y., and Hell, J.W. (2022). CaMKII: a central molecular organizer of synaptic plasticity, learning and memory. Nat. Rev. Neurosci. *23*, 666–682.

45. Sumi, M., Kiuchi, K., Ishikawa, T., Ishii, A., Hagiwara, M., Nagatsu, T., and Hidaka, H. (1991). The newly synthesized selective Ca^{2+}/calmodulin dependent protein kinase II inhibitor KN-93 reduces dopamine contents in PC12h cells. Biochem. Biophys. Res. Commun. *181*, 968–975.

46. Kurniawan, I.T., Guitart-Masip, M., and Dolan, R.J. (2011). Dopamine and effort-based decision making. Front. Neurosci. *5*, 81.

47. Rogers, R.D. (2011). The Roles of Dopamine and Serotonin in Decision Making: Evidence from Pharmacological Experiments in Humans. Neuropsychopharmacology *36*, 114–132.

48. Baik, J.H. (2021). Dopaminergic Control of the Feeding Circuit. Endocrinol. Metab. (Seoul) *36*, 229–239.

49. Beaulieu, J.M., and Gainetdinov, R.R. (2011). The Physiology, Signaling, and Pharmacology of Dopamine Receptors. Pharmacol. Rev. *63*, 182–217.

50. Kastenhuber, E., Kratochwil, C.F., Ryu, S., Schweitzer, J., and Driever, W. (2010). Genetic dissection of dopaminergic and noradrenergic

contributions to catecholaminergic tracts in early larval zebrafish. J. Comp. Neurol. *518*, 439–458.

51. Tay, T.L., Ronneberger, O., Ryu, S., Nitschke, R., and Driever, W. (2011). Comprehensive catecholaminergic projectome analysis reveals single-neuron integration of zebrafish ascending and descending dopaminergic systems. Nat. Commun. *2*, 171.
52. Randlett, O., Wee, C.L., Naumann, E.A., Nnaemeka, O., Schoppik, D., Fitzgerald, J.E., Portugues, R., Lacoste, A.M.B., Riegler, C., Engert, F., et al. (2015). Whole-brain activity mapping onto a zebrafish brain atlas. Nat. Methods *12*, 1039–1046.
53. Fernandes, A.M., Fero, K., Arrenberg, A.B., Bergeron, S.A., Driever, W., and Burgess, H.A. (2012). Deep Brain Photoreceptors Control Light-Seeking Behavior in Zebrafish Larvae. Curr. Biol. *22*, 2042–2047.
54. Doya, K. (2008). Modulators of decision making. Nat. Neurosci. *11*, 410–416.
55. Dragomir, E.I., Štih, V., and Portugues, R. (2020). Evidence accumulation during a sensorimotor decision task revealed by whole-brain imaging. Nat. Neurosci. *23*, 85–93.
56. Bahl, A., and Engert, F. (2020). Neural circuits for evidence accumulation and decision making in larval zebrafish. Nat. Neurosci. *23*, 94–102.
57. Shoenhard, H., Jain, R.A., and Granato, M. (2022). The calcium-sensing receptor (CaSR) regulates zebrafish sensorimotor decision making via a genetically defined cluster of hindbrain neurons. Cell Rep. *41*, 111790.
58. Jain, R.A., Wolman, M.A., Marsden, K.C., Nelson, J.C., Shoenhard, H., Echeverry, F.A., Szi, C., Bell, H., Skinner, J., Cobbs, E.N., et al. (2018). A Forward Genetic Screen in Zebrafish Identifies the G-Protein-Coupled Receptor CaSR as a Modulator of Sensorimotor Decision Making. Curr. Biol. *28*, 1357–1369.e5.
59. Preuss, S.J., Trivedi, C.A., vom Berg-Maurer, C.M., Ryu, S., and Bollmann, J.H. (2014). Classification of Object Size in Retinotectal Microcircuits. Curr. Biol. *24*, 2376–2385.
60. Niell, C.M., and Smith, S.J. (2005). Functional Imaging Reveals Rapid Development of Visual Response Properties in the Zebrafish Tectum. Neuron *45*, 941–951.
61. Förster, D., Helmbrecht, T.O., Mearns, D.S., Jordan, L., Mokayes, N., and Baier, H. (2020). Retinotectal circuitry of larval zebrafish is adapted to detection and pursuit of prey. eLife *9*, e58596.
62. Thanarajah, S.E., Backes, H., DiFeliceantonio, A.G., Albus, K., Cremer, A.L., Hanssen, R., Lippert, R.N., Cornely, O.A., Small, D.M., Brüning, J.C., et al. (2019). Food Intake Recruits Orosensory and Post-ingestive Dopaminergic Circuits to Affect Eating Desire in Humans. Cell Metab. *29*, 695–706.e4.
63. Lonze, B.E., and Ginty, D.D. (2002). Function and Regulation of CREB Family Transcription Factors in the Nervous System. Neuron *35*, 605–623.
64. Cox, J., and Mann, M. (2008). MaxQuant enables high peptide identification rates, individualized p.p.b.-range mass accuracies and proteome-wide protein quantification. Nat. Biotechnol. *26*, 1367–1372.
65. Cox, J., Hein, M.Y., Luber, C.A., Paron, I., Nagaraj, N., and Mann, M. (2014). Accurate Proteome-wide Label-free Quantification by Delayed Normalization and Maximal Peptide Ratio Extraction, Termed MaxLFQ. Mol. Cell. Proteomics *13*, 2513–2526.
66. Peirce, J., Gray, J.R., Simpson, S., MacAskill, M., Höchenberger, R., Sogo, H., Kastman, E., and Lindeløv, J.K. (2019). PsychoPy2: Experiments in behavior made easy. Behav. Res. Methods *51*, 195–203.
67. Kimura, Y., Satou, C., and Higashijima, S. (2008). V2a and V2b neurons are generated by the final divisions of pair-producing progenitors in the zebrafish spinal cord. Development *135*, 3001–3005.
68. Thiele, T.R., Donovan, J.C., and Baier, H. (2014). Descending Control of Swim Posture by a Midbrain Nucleus in Zebrafish. Neuron *83*, 679–691.
69. Asakawa, K., Suster, M.L., Mizusawa, K., Nagayoshi, S., Kotani, T., Urasaki, A., Kishimoto, Y., Hibi, M., and Kawakami, K. (2008). Genetic dissection of neural circuits by *Tol2* transposon-mediated Gal4 gene and enhancer trapping in zebrafish. Proc. Natl. Acad. Sci. USA *105*, 1255–1260.
70. Gagnon, J.A., Valen, E., Thyme, S.B., Huang, P., Akhmetova, L., Pauli, A., Montague, T.G., Zimmerman, S., Richter, C., and Schier, A.F. (2014). Efficient Mutagenesis by Cas9 Protein-Mediated Oligonucleotide Insertion and Large-Scale Assessment of Single-Guide RNAs. PLoS One *9*, e98186.
71. Gibson, U.E., Heid, C.A., and Williams, P.M. (1996). A novel method for real time quantitative RT-PCR. Genome Res. *6*, 995–1001.
72. Corradi, L., Zaupa, M., Sawamiphak, S., and Filosa, A. (2022). Using pERK immunostaining to quantify neuronal activity induced by stress in zebrafish larvae. Star Protoc. *3*, 101731.
73. Lister, J.A., Robertson, C.P., Lepage, T., Johnson, S.L., and Raible, D.W. (1999). nacre encodes a zebrafish microphthalmia-related protein that regulates neural-crest-derived pigment cell fate. Development *126*, 3757–3767.
74. Pnevmatikakis, E.A., and Giovannucci, A. (2017). NoRMCorre: An online algorithm for piecewise rigid motion correction of calcium imaging data. J. Neurosci. Methods *291*, 83–94.
75. Miri, A., Daie, K., Burdine, R.D., Aksay, E., and Tank, D.W. (2011). Regression-Based Identification of Behavior-Encoding Neurons During Large-Scale Optical Imaging of Neural Activity at Cellular Resolution. J. Neurophysiol. *105*, 964–980.
76. Lovett-Barron, M., Andalman, A.S., Allen, W.E., Vesuna, S., Kauvar, I., Burns, V.M., and Deisseroth, K. (2017). Ancestral Circuits for the Coordinated Modulation of Brain State. Cell *171*, 1411–1423.e17.
77. Jefferis, G. (2012). IGS (CMTK) Image Registration Tools Classic MacOSX GUI. Zenodo. https://zenodo.org/records/1193268.

Please cite this article in press as: Zaupa et al., The Calmodulin-interacting peptide Pcp4a regulates feeding state-dependent behavioral choice in zebrafish, Neuron (2024), https://doi.org/10.1016/j.neuron.2024.01.001

STAR★METHODS

KEY RESOURCES TABLE

REAGENT or RESOURCE	SOURCE	IDENTIFIER
Antibodies		
Chicken polyclonal anti-GFP	Thermo Fisher	Cat# A10262; RRID: AB_2534023
Mouse monoclonal anti- p44/42 MAPK	Cell Signaling	Cat# 4696; RRID: AB_390780
Rabbit monoclonal anti- phospho-p44/42 MAPK (Thr202/Tyr204)	Cell Signaling	Cat# 4370; RRID: AB_2315112
Goat polyclonal anti-chicken IgY, Alexa Fluor 488 conjugate	Thermo Fisher	Cat# A11039; RRID: AB_142924
Goat polyclonal anti-mouse IgG, Alexa Fluor 647 conjugate	Cell Signaling	Cat# 4410; RRID: AB_1904023
Goat anti-rabbit IgG, Alexa Fluor 555 conjugate	Cell Signaling	Cat# 4413; RRID: AB_10694110
Chemicals, peptides, and recombinant proteins		
Trypsin-EDTA	Sigma	Cat# T4299
Agarose, Low Melting Point	Roboklon	E0303-50
Tricaine (3-amino benzoic acidethylester)	PHARMAQ	N/A
Dimethyl sulfoxide (DMSO)	Th. Geyer	Cat# 23419.3
Pancuronium bromide	Sigma	Cat# P1918
Triton X 100	Roth	Cat# 3051.3
Tween 20	Roth	Cat# 9127.2
Bovine Serum Albumin	Serva	Cat# 11943.02
Paraformaldehyde (PFA)	Sigma	Cat# P6148
Goat serum	Sigma	Cat# G6767
Proteinase K	Sigma	Cat# 3115879001
Fluoxetine hydrochloride	Sigma	Cat# PHR1394
Donepezil hydrochloride	Thermo Fisher	Cat# 458050010
Apomorphine hydrochloride	AbCam	Cat# ab269887
SKF-38393 hydrochloride	MedChem Express	Cat# HY-12520A
Quinpirole hydrochloride	Sigma	Cat# Q102
Forskolin	Sigma	Cat# F6886
KN-93	Adooq Bioscience	Cat# A13276
Trizol	Thermo Fisher	Cat# 15596026
DNase I	Thermo Fisher	Cat# EN0521
Critical commercial assays		
HCRv3 reagents	Molecular Instruments	https://www.molecularinstruments.com/
Superscript III First-Strand Synthesis kit	Life Technologies	Cat# 18080051
Luna Universal qPCR Master Mix	New England BioLabs	Cat# M3003L
Deposited data		
Whole-larva proteome from 7dpf fed zebrafish larvae and non-fed clutchmates	This paper	MassIVE: MSV000091374 https://doi.org/10.25345/C50P0X15F
Experimental models: Organisms/strains		
Zebrafish: *Tg[elavl3:H2B-GCaMP6s]*^{jf5}	Freeman et al.[40]	ZFIN: ZDB-ALT-141023-2
Zebrafish: *Tg[elavl3:GAL4-VP16]*^{nn6Tg}	Kimura et al.[64]	ZFIN: ZDB-ALT-090116-2
Zebrafish: *Tg[14XUAS:GCaMP6s]*^{mpn101}	Thiele et al.[65]	ZFIN: ZDB-ALT-140811-3
Zebrafish: *Tg[-7atoh7:GAL4-VP16]*^{s1992t}	Del Bene et al.[42]	ZFIN: ZDB-ALT-110912-2
Zebrafish: *Tg[5XUAS:EGFP]*^{nkuasgfp1a}	Asakawa et al.[66]	ZFIN: ZDB-ALT-080528-1

(*Continued on next page*)

Continued

REAGENT or RESOURCE	SOURCE	IDENTIFIER
Zebrafish: *Tg[th:GAL4-VP16]*^{m1233}	Fernandes et al.[54]	ZFIN: ZDB-ALT-130110-4
Zebrafish: *Tg[UAS:EGFP-CAAX]*^{m1230}	Fernandes et al.[54]	ZFIN: ZDB-ALT-130110-5
Zebrafish: *pcp4a*^{md78}	This paper	N/A
Oligonucleotides		
sgRNA *pcp4a*^{md78}: GGAAGCATCAAACCCTCAGGTGG	This paper	N/A
Primer: genotyping *pcp4a* Forward GAAAACAGACATCCCCGCTGTG	This paper	N/A
Primer: genotyping *pcp4a* Reverse CCCCCACAAATCCAAAGACGTG	This paper	N/A
Primer: qPCR *pcp4a* Forward CTCAGGTGGACAAGACCCATC	This paper	N/A
Primer: qPCR *pcp4a* Reverse ATCCCCCTGCCCTAAATGTG	This paper	N/A
Primer: qPCR *β-actin* Forward GTCCCTGTATGCCTCTGGT	This paper	N/A
Primer: qPCR *β-actin* Reverse AAGTCCAGACGGAGGATG	This paper	N/A
Software and algorithms		
Maxquant version 2.2.0.0	Max-Planck-Institute of Biochemistry	www.maxquant.org
Perseus 2.0.7.0	Max-Planck-Institute of Biochemistry	https://maxquant.net/perseus/
Fiji/ImageJ	NIH	https://fiji.sc/
Prism version 9	GraphPad Software	https://www.graphpad.com/scientific-software/prism/
EthoVision XT version 8.5	Noldus	https://www.noldus.com/ethovision-xt
MATLAB	The MathWorks	https://www.mathworks.com/products/matlab.html
Imaris version 10	Oxford Instruments	https://imaris.oxinst.com/
PsychoPy version 2.0	Open Science Tools	https://www.psychopy.org/
Python code for size discrimination behavioral assay	This paper	https://doi.org/10.5281/zenodo.8410018
Python code for visual stimulation for calcium imaging	This paper	https://doi.org/10.5281/zenodo.8410018
Python code for optomotor response assay	This paper	https://doi.org/10.5281/zenodo.8410018
Other		
Camera	XIMEA	Cat# MQ003MG-CM
Infrared filter	Thorlabs	Cat# FGL7806S
StepOnePlus Real-Time PCR System	Applied Biosystem	Cat# 4376600

RESOURCE AVAILABILITY

Lead contact

Further information and requests for resources and reagents should be directed to the lead contact, Alessandro Filosa (alessandro.filosa@mdc-berlin.de).

Materials availability

The *pcp4a*^{md78} zebrafish line is available upon request.

Data and code availability

- Mass spectrometry data have been deposited at MassIVE and are publicly available as of the date of publication. The accession number is listed in the key resources table. Other data reported in this paper will be shared by the lead contact upon request.

- All original code has been deposited at Zenodo and is publicly available as of the date of publication. DOIs are listed in the key resources table.
- Any additional information required to reanalyze the data reported in this paper is available from the lead contact upon request.

EXPERIMENTAL MODEL AND STUDY PARTICIPANT DETAILS

Zebrafish lines and maintenance

Zebrafish were kept under standard conditions at 28.5°C on a 14 hr/10 hr light/dark cycle. Embryos and larvae were kept in Danieau's medium (58 mM NaCl, 0.7 mM KCl, 0.4 mM $MgSO_4$, 0.6 mM $Ca(NO_3)_2$, 5 mM HEPES, pH adjusted to 7) at a density of approximately 40 fish in a 90 mm plastic Petri dish. Unless otherwise stated, experiments were performed at 7 dpf. All animal procedures were conducted in accordance with institutional (Max Delbrück Center for Molecular Medicine, and Max Planck Institute for Biological Intelligence), State (LAGeSo Berlin, and Regierung Oberbayern), and German ethical and animal welfare guidelines and regulations, and according to protocols approved by LAGeSo. Larvae were euthanized, following anesthesia with tricaine, using hypothermic exposure (ice bath) for 20 minutes. Sex of zebrafish cannot be determined at the developmental stages considered in this study. Animals were randomly assigned to experimental groups. The following previously established transgenic lines were used in this study: *Tg[elavl3:H2B-GCaMP6s]*[jf5],[40] *Tg[elavl3:Gal4]*[nn6Tg],[67] *Tg[14XUAS:GCaMP6s]*[mpn101],[68] *Tg[atoh7:Gal4]*[s1992t],[42] *Tg[5XUAS:EGFP]*[nkuasgfp1a],[69] *Tg[th:Gal4-VP16]*[m1233],[53] *Tg[UAS:EGFP-CAAX]*[m1230].[53]

The *pcp4a*[md78] mutant line was generated using the CRISPR/Cas9 technique. A guide RNA (5'-GGAAGCATCAAACCCT-CAGGTGG-3') targeting exon 2 of *pcp4a* was synthesized following an established protocol.[70] The sgRNA (100 ng/μl) and Cas9 protein (600 ng/μl) were injected in wild type embryos at one-cell stage. Founders were selected for an 8 bp deletion leading to a frameshift mutation and formation of a premature stop codon in exon 3.

For genotyping fish, the genomic region containing the *pcp4a*[md78] mutation was amplified by PCR using the primers 5'-GAAAA CAGACATCCCCGCTGTG-3' and 5'-CCCCCACAAATCCAAAGACGTG-3', which in wild types produce a 632 bp DNA fragment. After digestion with the restriction enzyme DdeI (New England BioLabs, Cat# R0175L), the DNA fragment amplified from the wild-type allele produces 2 bands of 484 bp and 148 bp. Since the mutant allele is missing the DdeI restriction site, an uncut band of 624 bp is produced.

METHOD DETAILS

Feeding protocol

At 5 dpf, siblings were split in 90 mm Petri dishes with Danieau's medium at approximately 40 fish per dish. Larvae in the fed groups were fed one time at 5 dpf and two times per day from 6 dpf with dry food (SDS-100, Special Diets Services). The medium was changed prior to each feeding. Fish in the food-deprived groups did not receive food, and the medium was changed with the same timing and frequency as in the fed groups. Prior to experiments, gut content was inspected under a stereomicroscope to ensure that fish in the fed groups ingested food.

Mass spectrometry

To obtain each sample for mass spectrometry analysis, we pooled ten 7 dpf larvae (either fed or not fed). After euthanasia, larvae were transferred into 1.5 ml microcentrifuge tubes. Water was removed from the tubes, and the larvae were fast-frozen with liquid nitrogen and stored at -80°C. After thawing them on ice, the samples were re-suspended in 20 μl of 6 M guanidium hydrochloride in 25 mM Tris buffer containing 10 mM tris(2-carboxyethyl)phosphine (TCEP) and 40 mM chloroacetamide, pH 8.0. The samples were then heated at 95°C for two minutes and sonicated using a Bioruptor sonicator (Diagenode) for ten minutes at maximum power for ten cycles. The heating and sonication steps were repeated twice to ensure complete lysis of the samples. Afterward, the samples were incubated for 30 minutes at 37°C, diluted in 200 μl of 20 mM ammonium bicarbonate solution, and then incubated with 1 μg of Trypsin (Promega) for overnight digestion. The digested peptides were purified on a 3 plug C18 StageTip (ThermoFisher) and loaded into a Q Exactive orbitrap mass spectrometer (ThermoFisher).

Raw data were processed in Maxquant version 2.2.0.0[64] using UniProt fasta database from *Danio rerio*. Database searching was performed with initial mass deviation of 7 ppm and all identifications were filtered at 1 % for protein and peptide level. Match between the runs option was enabled and label-free quantification was performed using the MaxLFQ algorithm.[65] Protein groups file was then analyzed using Perseus 2.0.7.0 to perform two sample t tests. Differences of protein amounts were considered significant if the False Discovery Rate (FDR) was lower than 0.05. Protein functions indicated in Table S1 were obtained from UniProt (www.uniprot.org) and the Zebrafish Information Network (https://zfin.org).

Behavioral assays

The behavioral setup was positioned on a vibration isolation table and shielded from external illumination. The light source was a computer screen placed underneath the recording arena. Fish were imaged using a high-speed camera (Ximea) placed above the chambers containing the larvae.

Spontaneous locomotion was first measured. One hour prior to the experiment, fish were transferred to a 12-wells plate containing 2 ml of Danieau's medium in each well, which was then placed in the behavior-recording setup 10 minutes before the start of the experiment. Spontaneous locomotion was then imaged for 10 minutes at 40 Hz. The software Ethovision XT 8.5 was then used to track the fish trajectories and calculate the total distance travelled by each larva.

To measure behavioral choice, a previously established visual size discrimination assay was used.[29,30] Individual larvae were placed in custom-made transparent plastic chambers (100 X 12 mm) containing 4 ml of Danieau's medium, and black circles of different sizes (1° to 30° of visual angle) moving at a constant speed of 33°/s were showed on a display with white background underneath the fish. Visual stimuli were generated using PsychoPy v2.0[66] with a custom-written script. Circle sizes were calculated as the degrees of the visual field, occupied by the stimulus positioned right below a larva. Since the fish were freely moving, the entire set of stimuli was repeated five times, with two-minutes intervals between each set to maximize the number of stimulus-larva interactions. Locomotor responses to the visual stimuli were imaged at 60 Hz, and subsequently manually scored as approaches (if the larvae swam toward an approaching visual stimulus with at least one swimming bout), avoidances (if the larvae swam away from an approaching stimulus with at least one swimming bout), or neutral interactions (when the larvae swam neither toward to or away from stimuli) by an expert investigator blind to the identity of the experimental groups.

To quantify the tendency of fish to approach or avoid circles, a valence index [(approaches – avoidances) / (approaches + avoidances)] was used, which is equal to 1 if 100% of the interactions are approaches, and to –1 if they are 100% avoidances. To quantify the general efficiency of larva-stimulus interactions, an activity index [(approaches + avoidances) / (approaches + avoidances + neutral interactions)] was calculated. The activity index is equal to 0 if 100% of the interactions are neutral, and to 1 if none of them are neutral.

The optomotor response assay was performed on 5 dpf head-fixed larvae. Larvae were mounted in a 6 cm petri dish in 2% low-melting point agarose and covered with Danieau's buffer. The agarose was cut below the swimming bladder to free the tail. Black and white gratings with bars of different size (1° to 10° of visual angle) moving forward at a constant speed of 60°/s were displayed on a screen underneath the fish, and the optomotor response of the fish was recorded for 30 seconds. Larvae were illuminated from above with a custom-built infrared LED ring. An infrared filter (780 nm LP, Thorlabs, Cat#FGL7806S) was placed in front of the camera to block visible light coming from the screen displaying moving bars. Locomotor responses to the moving bars were imaged at 250 Hz. Amplitude and duration of swimming bouts were manually measured using ImageJ. Attempts of the fish to free itself from the agarose ('struggles') were distinguished from swimming bouts based on the tail angle (> 90°) and were not included in the analysis.

qRT–PCR

After euthanizing the larvae, their brains were manually dissected using fine dissection forceps (Dumont) in a 35 mm Petri dish containing ice-cold PBS, which bottom was coated with 5% agarose in PBS. Ten brains were pooled for each sample. For the group treated with forskolin, and the related control group, ten whole 5 dpf larvae were pooled for each sample. Samples were mechanically homogenized in Trizol and stored at -80°C. Total RNA was extracted by chloroform purification followed by isopropanol precipitation. DNase I treatment was used to prevent genomic DNA contamination, and RNA quality was checked using a Nanodrop spectrophotometer (Eppendorf). cDNA was synthesized using the Superscript III First-Strand Synthesis kit (Life Technologies, Cat# 18080051) using oligodT primers, and RNase H treatment was used to digest the RNA template.

qRT–PCR was performed using Luna Universal qPCR Master Mix (New England BioLabs, Cat# M3003L) in a StepOnePlus Real-Time PCR System (Applied Biosystem). *pcp4a*'s mRNA was amplified using the primers 5'-CTCAGGTGGACAAGACCCATC-3' and 5'-ATCCCCCTGCCCTAAATGTG-3'. Each biological replica was run in triplicate, 10 ng of cDNA were used for each reaction. The housekeeping *β-actin* mRNA was used as endogenous control (using the primers 5'-GTCCCTGTATGCCTCTGGT-3' and 5'-AAGTC CAGACGGAGGATG-3' for its amplification). For each biological replica, two pools of brains or larvae from the same clutch of fish were collected, one to be subjected to experimental treatment and one as a control for normalization of gene expression using the $2^{-\Delta\Delta Ct}$ method.[71] Different biological replicas were obtained from different clutches.

In situ hybridization

In situ hybridization to detect *pcp4a*, *vglut2*, *gad1b*, *drd2a*, and *drd2b* transcripts was performed using third-generation *in situ* HCR v.3.0.[41] All the probes and fluorophore-conjugated hairpins were purchased from Molecular Instruments Inc. *vglut2* probes recognized both zebrafish *vglut2* paralogs *slc17a6a* and *slc17a6b*. *In situ* HCR v.3.0 was performed following the manufacturer's protocol, taking care of keeping the fish always in the dark to preserve endogenous fluorescence signal. Briefly, larvae were fixed overnight in 4% PFA in PBS and then incubated in 100% methanol at -20°C for at least 10 min. After rehydration in PBT (PBS + 0.1% Tween20), larvae were permeabilized with proteinase K (10 μg/ml) for 15-30 min, followed by postfixation in 4% PFA. Larvae were then incubated in probe hybridization buffer (Molecular Instruments Inc.) with 4 nM of each probe at 37°C overnight. After washes at 37°C, larvae were incubated overnight in amplification buffer (Molecular instruments Inc.) with 30 nM of each fluorophore-conjugated hairpin at room temperature. After washing in 5X SSCT, larvae were immediately mounted in 1.5% low-melting-point agarose and imaged with a Leica DM6 CFS confocal microscope with a 25X water-immersion objective (HC Fluotar L 25X/0.95, Leica Microsystems). Volume rendering of confocal stacks of the tectum and mapping of position of *pcp4a*+ PVNs was performed with the software Imaris.

Please cite this article in press as: Zaupa et al., The Calmodulin-interacting peptide Pcp4a regulates feeding state-dependent behavioral choice in zebrafish, Neuron (2024), https://doi.org/10.1016/j.neuron.2024.01.001

Immunohistochemistry

Immunohistochemistry was performed following an established protocol.[72] Larvae were fixed overnight in 4% PFA in PBST (PBS with 0.3% Triton) at 4°C. They were then washed in PBST, and incubated in 150 mM Tris-HCl (pH = 9) for 5 minutes at room temperature, followed by 15 minutes at 70°C. Afterward, larvae were incubated in Trypsin EDTA (Sigma, Cat# T4299, diluted 1:20 in PBST) for 40 minutes on ice. After 1 hour of blocking at room temperature in blocking solution (5% goat serum, 1% BSA, 1% DMSO in PBST), fish were incubated with primary antibodies, each diluted 1:500 in blocking solution for 96 hours at 4°C. Larvae were then washed in PBST, incubated in blocking solution for 1 hour at room temperature, and then with Alexa Fluor secondary antibodies, each diluted 1:300 in blocking solution for 48 hours at 4°C. Primary antibodies against the following antigens were used: GFP (Invitrogen, Cat# A10262), total ERK (tERK; Cell Signaling, Cat# 4696), phosphorylated ERK (pERK; Cell Signaling, Cat# 4370). The following Alexa Fluor secondary antibodies were used: α-chicken-AF488 (ThermoFisher, Cat# A11039), α-mouse-AF647 (Cell Signaling, Cat# 4410S), α-rabbit-AF555 (Cell Signaling, Cat# 4413S). Images of the samples were acquired using a Leica DM6 CFS confocal microscope with a 25X water-immersion objective (HC Fluotar L 25X/0.95, Leica Microsystems). All larvae were imaged using constant acquisition settings. GFP-positive cells in *th:gal4-VP16; UAS:EGFP-CAAX* larvae were manually selected to measure the fluorescent intensities of pERK and tERK immunostainings using ImageJ. The cumulative percentage of pERK/tERK values was calculated for each larva and then averaged across fish.

Pharmacology

Wild-type clutchmate larvae were equally split into two different Petri dish just before drug application. The following treatments were used: 1.5 μM fluoxetine hydrochloride (Sigma, Cat# PHR1394) for 4 hours, 10 μM donepezil hydrochloride (Fisher, Cat# 458050010) with 0.1% DMSO for 24 hours, 50 μM apomorphine hydrochloride (AbCam, Cat# ab269887) with 0.1% DMSO for 2 hours, 50 μM SKF-38393 hydrochloride (MedChem Express, Cat# HY-12520A) with 0.1% DMSO for 4 hours, 16.7 μM quinpirole hydrochloride (Sigma, Cat# Q102) with 0.1% DMSO for 3 hours, 10 μM forskolin (Sigma, Cat# F6886) with 0.1% DMSO for 1 hour. Control groups were incubated in Danieau's medium with 0.1% DMSO, with the exception of the control group for fluoxetine treatment, which was incubated only in Danieau's medium.

For the treatment combining quinpirole with forskolin, fish were first incubated in 16.7 μM quinpirole hydrochloride with 0.1% DMSO. After two hours, 10 μM forskolin with 0.1% DMSO was added to the medium. Fish were incubated in both drugs for one additional hour.

Calcium imaging

Fish used for Ca^{2+} imaging were homozygous *mitfa*$^{w2/w2}$ mutants lacking skin melanophores.[73] Larvae were mounted in 1% low-melting-point agarose containing the myorelaxant pancuronium bromide (0.3 mg/ml, Sigma, Cat# P1918) to minimize fish movement, in a petri Dish filled with Danieau's medium. Black circles of different sizes (1° to 30° of visual angle), moving at a constant speed (4.4°/s) on a grey background, were displayed on a microdisplay (Kopin) on one side of the fish. Responses to the visual stimuli were imaged in the contralateral side of the tectum using a confocal microscope (Zeiss LSM 880 NLO) equipped with a 20X water-immersion objective (W Plan Apochromat 20X/1.0 DIC VIS-IR, Zeiss). Time series were acquired at 4 Hz with a pixel size of 1 μm^2. Three to four z-planes were acquired for each fish at different depths in the tectum.

Raw images were first x-y motion corrected using the NoRMCorre algorithm in Matlab.[74] Region of interests (ROIs) corresponding to single neurons were drawn manually. GCaMP6s fluorescence intensity was normalized as $\Delta F/F_0 = (F - F_0) / F_0$ where F is the fluorescence at each time point and F_0 is the average baseline fluorescence (10 frames preceding the stimulus presentation). A neuron was considered responding to a stimulus if the calcium peak was higher than two standard deviations of the baseline. The size tuning of neurons was expressed as WMR angles, calculated as weighted sums of visual stimulus sizes, to which neuronal responses were non-zero:

$$\mathrm{WMRangle} = \sum_{i=1}^{n} w_i * x_i$$

where x_i are the angular sizes of the visual stimuli and w_i are the weights calculated as

$$w_i = \left(\frac{\Delta F}{F_0}\right) i \Big/ \sum_{i=1}^{n} \left(\frac{\Delta F}{F_0}\right) i$$

To analyze responses to visual stimuli in the tectal neuropil, a pixel-wise analysis based on a regression model was performed.[30,75] A linear regression model composed of six independent variables corresponding to the individual responses for the different visual stimulus sizes, and by a constant term, was used to represent the temporal series for each pixel. The regressor functions were obtained from the convolution of the waveforms of the stimulus presence with a GCaMP6s kernel, whose t_{off} = 1.8 s was based on the coefficient of determination R^2. The distributions of T scores for different sizes of the stimuli were averaged across different trials (Figure S4H). Corrected distributions were obtained by subtracting a term equal to 3 SD, accounting for changes in fluorescence in absence of stimulation. The number of pixels activated by the presentation of visual stimuli (Figure S4G) was quantified by calculating the integrals of the corrected distributions.

Neurons expressing *pcp4a* were identified *post mortem* using an approach similar to the MultiMAP method.[76] After recording activity of tectal neurons with Ca^{2+} imaging in a selected set of z-planes, a stack of images of the whole tectum contralateral to the eye receiving visual stimulation was acquired with a 1 μm z-step. Minimal x-y shifts between the same plane in the Ca^{2+} imaging time-lapse and in the stack were manually corrected in ImageJ using the 'translate' function to ensure accurate cell identification. Immediately after imaging, the fish were euthanized and fixed in 4% PFA, and *in situ* HCR was performed to detect *pcp4a*'s mRNA using the protocol described above. Then a stack of images of the same tectum with the residual GCaMP6s fluorescence and the *pcp4a in situ* HCR signal was acquired with 1 μm z-step. The two stacks from each larva were then aligned with each other, using the GCaMP6s fluorescence in the two data sets to guide the alignment, with the CMTK plugin in Fiji.[77] The z-planes containing the neurons whose activity was recorded during the *in vivo* calcium imaging session were identified in the registered stack and the accuracy of the registration was checked manually. Neurons were considered positive for *pcp4a* if the *in situ* signal occupied at least 50% of the perimeter of the nuclei labeled by H2B-GCaMP6s. In case of uncertainty, z-planes below and above the imaging plane were checked in the registered stack.

For the experiments testing the effect of dopaminergic D2-like receptor signaling on the activity of *pcp4a*+ PVNs, responses to visual stimuli were first recorded using *in vivo* calcium imaging as described above. The fish, still embedded in agarose, were then incubated for 3 hours in Danieau's medium containing 16.7 μM quinpirole hydrochloride (Sigma, Cat# Q102) or in Danieau's medium as a control. Larvae were then transferred again under the microscope, with the drug still in the solution, and responses to visual stimuli were recorded a second time from the same z-planes containing the PVNs imaged during the first session. *Post mortem* identification of *pcp4a*+ neurons and analyses of GCaMP6s signal were then performed as described above.

For the experiment testing the effect of CaMKII inhibition on the activity of *pcp4a*+ PVNs, fish were first treated with the CaMKII inhibitor KN93 (5 μM, Adooq Bioscience, Cat#A13276-5) with 0.1% DMSO or Danieau's medium with 0.1% DMSO for 3 hours prior to experiment. Responses to visual stimuli were recorded using calcium imaging as described above with the drug still in the solution.

QUANTIFICATION AND STATISTICAL ANALYSIS

Statistical significance was determined using one-sample t tests, two-tailed Student's t tests, two-way ANOVA, and nested two-way ANOVA in GraphPad Prism (GraphPad, version 9). Normal distribution of data was verified with the Shapiro-Wilk test before performing t tests or ANOVA. p values from multiple Student's t tests were corrected using the Bonferroni-Holm method. Statistical tests were considered significant if $p < 0.05$.

Neuron, Volume *112*

Supplemental information

The Calmodulin-interacting peptide Pcp4a regulates feeding state-dependent behavioral choice in zebrafish

Margherita Zaupa, Nagarjuna Nagaraj, Anna Sylenko, Herwig Baier, Suphansa Sawamiphak, and Alessandro Filosa

Supplemental Information

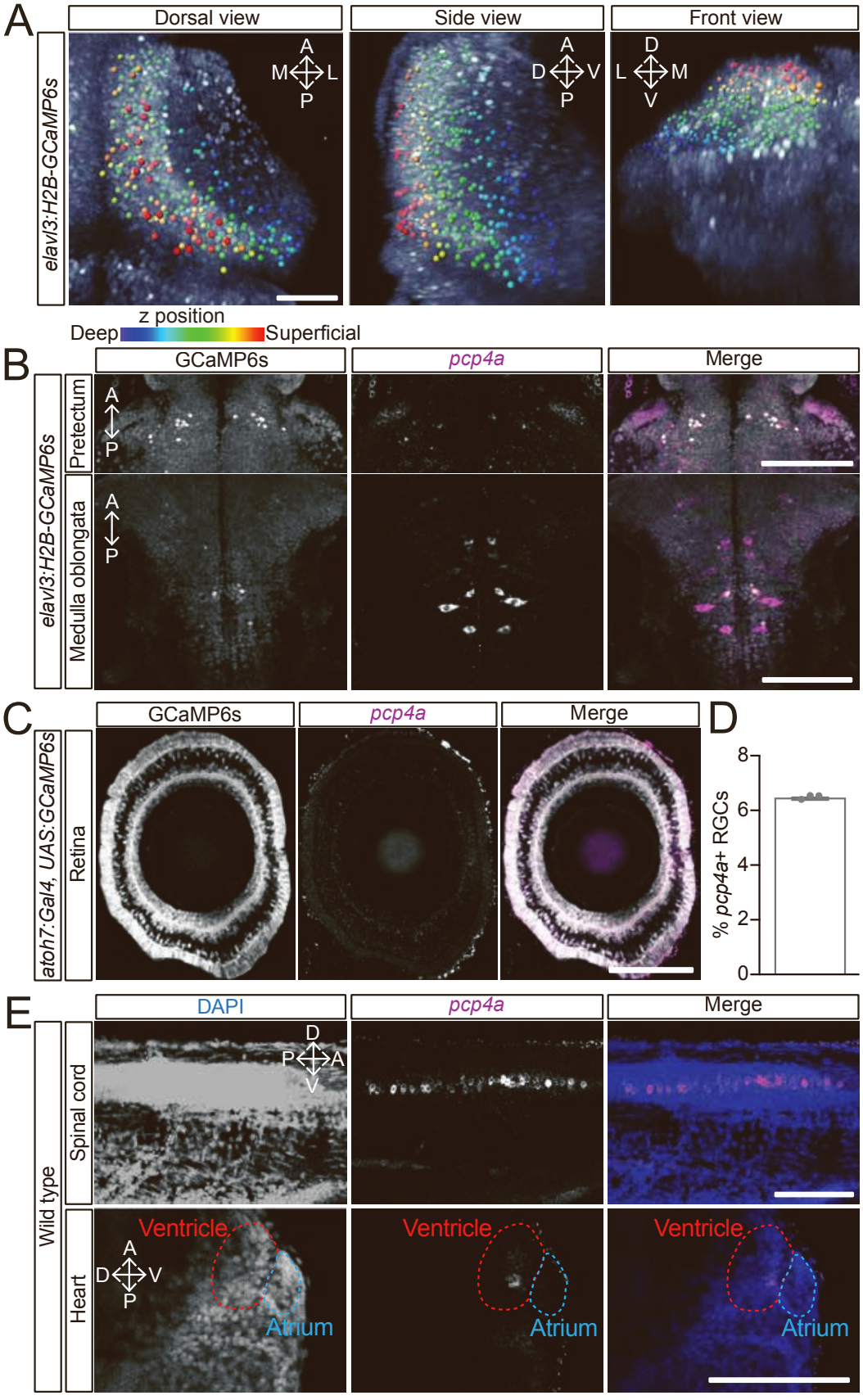

Figure S1. Localization of *pcp4a*+ cells inside and outside the central nervous system. Related to Figure 1. **A.** Top, side, and front views of a 3D-rendered volume of the tectum of a 7 dpf *elavl3:H2B-GCaMP6s* larva. Spheres indicate *pcp4a*+ PVNs identified by *in situ* HCR, and color-coded according to depth. **B, C.** Confocal images showing localization of the mRNA coding for Pcp4a in the pretectum and medulla oblongata of 7 dpf *elavl3:H2B-GCaMP6s* fish (B), and in the retina of a 7 dpf *atoh7:gal4, UAS:GCaMP6s* larva (C). **D.** Graph depicting average percentage of *pcp4a*+ RGCs in the retina. Data are shown as mean ± standard error of the mean. n = 3 larvae. **E.** Confocal images displaying expression of *pcp4a* in the ventral spinal cord and heart of 7 dpf wild-type fish. Outside the central nervous system, Pcp4a-coding mRNA was detectable only in the heart. Scale bars, 50 μm (A), 100 μm (B, C, E). Abbreviations: A, anterior; D, dorsal; L, lateral; M, medial; P, posterior; V, ventral.

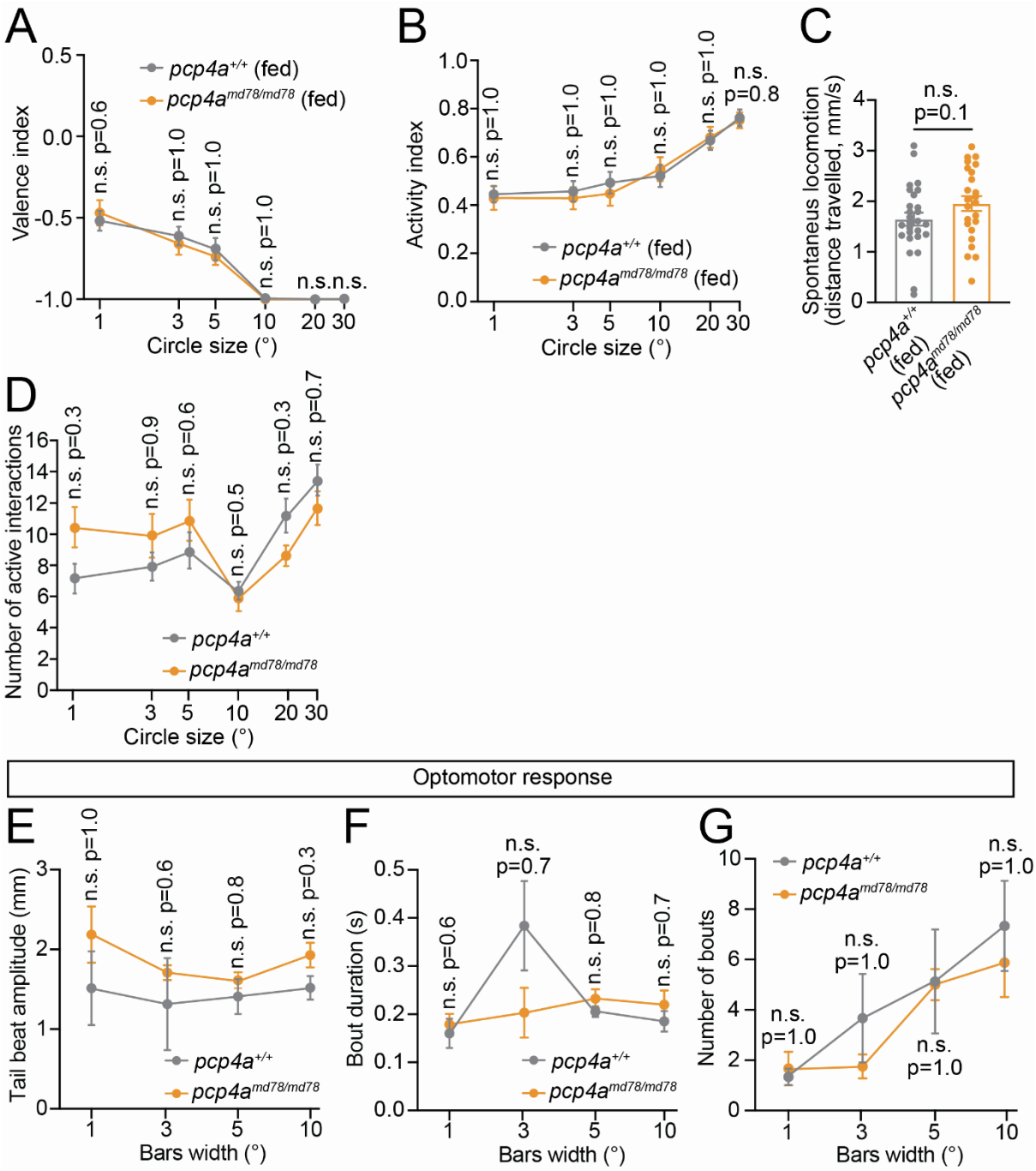

Figure S2. Behavioral performance of *pcp4a* mutants. Related to Figure 2. **A, B.** Graphs depicting average valence indexes (A) or activity indexes (B) for different sizes of visual stimuli of 7 dpf fed *pcp4a*$^{+/+}$ and *pcp4a*$^{md78/md78}$ larvae. $n_{pcp4a+/+}$ = 26 larvae, $n_{pcp4amd78/md78}$ = 22 larvae. **C.** Bar graph showing average spontaneous locomotion of 7 dpf fed *pcp4a*$^{+/+}$ and *pcp4a*$^{md78/md78}$ larvae. $n_{pcp4a+/+}$ = 27 larvae, $n_{pcp4amd78/md78}$ = 24 larvae. **D.** Graph displaying average number of active interactions (approaches + avoidances) in 7 dpf fed *pcp4a*$^{+/+}$ and *pcp4a*$^{md78/md78}$ fish. $n_{pcp4a+/+}$ = 22 larvae, $n_{pcp4amd78/md78}$ = 18 larvae. **E – G.** Graphs showing tail beat amplitude (E), bout duration (F), and number of bouts during optomotor responses performed by 5 dpf unfed *pcp4a*$^{+/+}$ and *pcp4a*$^{md78/md78}$ fish. $n_{pcp4a+/+}$ = 10 larvae, $n_{pcp4amd78/md78}$ =

9 larvae. Data are shown as mean ± standard error of the mean. n.s., not significant. Statistical significance was tested using two-tailed t test with Bonferroni-Holm correction, with the exception of the dataset shown in (C), in which correction for multiple comparisons was not applied.

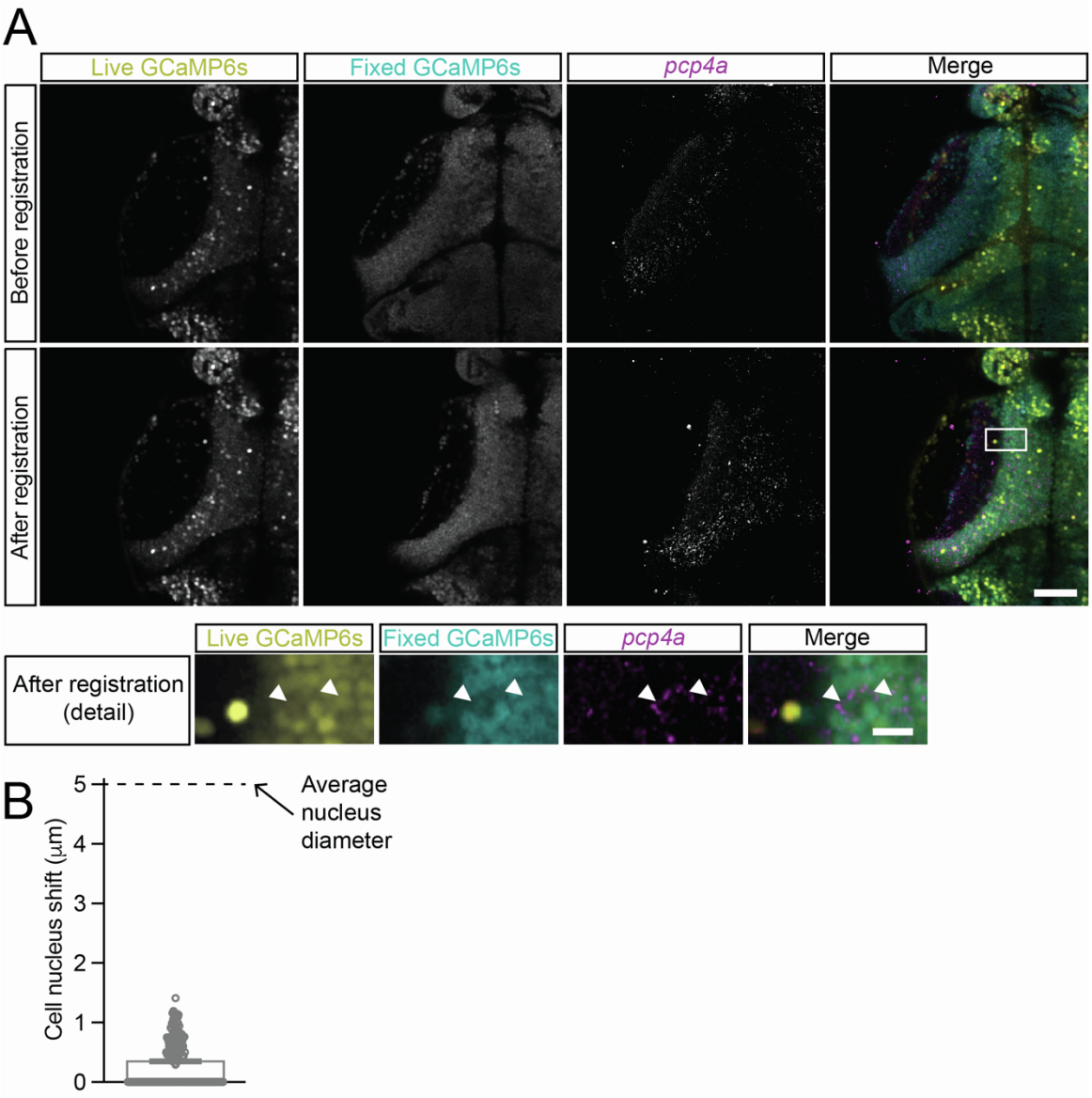

Figure S3. Registration of *in vivo* and *post mortem* confocal images following Ca^{2+} imaging and *in situ* HCR. Related to Figure 3. **A.** Images showing GCaMP6s signal before (live GCaMP6s, average projections of a Ca^{2+} imaging timelapse of a single z-plane) and after fixation (fixed GCaMP6s, corresponding z-plane of the fixed and stained sample), and *pcp4a*'s mRNA localization (detected by *in situ* HCR) in a 7 dpf *elavl3:H2B-GCaMP6s* larva, before and after registration of the *in vivo* and fixed confocal images. At the bottom, high magnification images of the area marked by the white rectangle in the top panel are shown. Scale bars, 50 μm (top panel) or 10 μm (bottom panel). Note that registration of the periventricular layer is very efficient, while the neuropil region of the two images does not align well. **B.** Graph depicting quantification of shift of cell nuclei between the *in vivo* and *post mortem* images after registration. The average shift was minimal, compared to the average cell nucleus diameter. n = 168 randomly selected neurons from 3 fish. Data are shown as mean ± standard error of the mean.

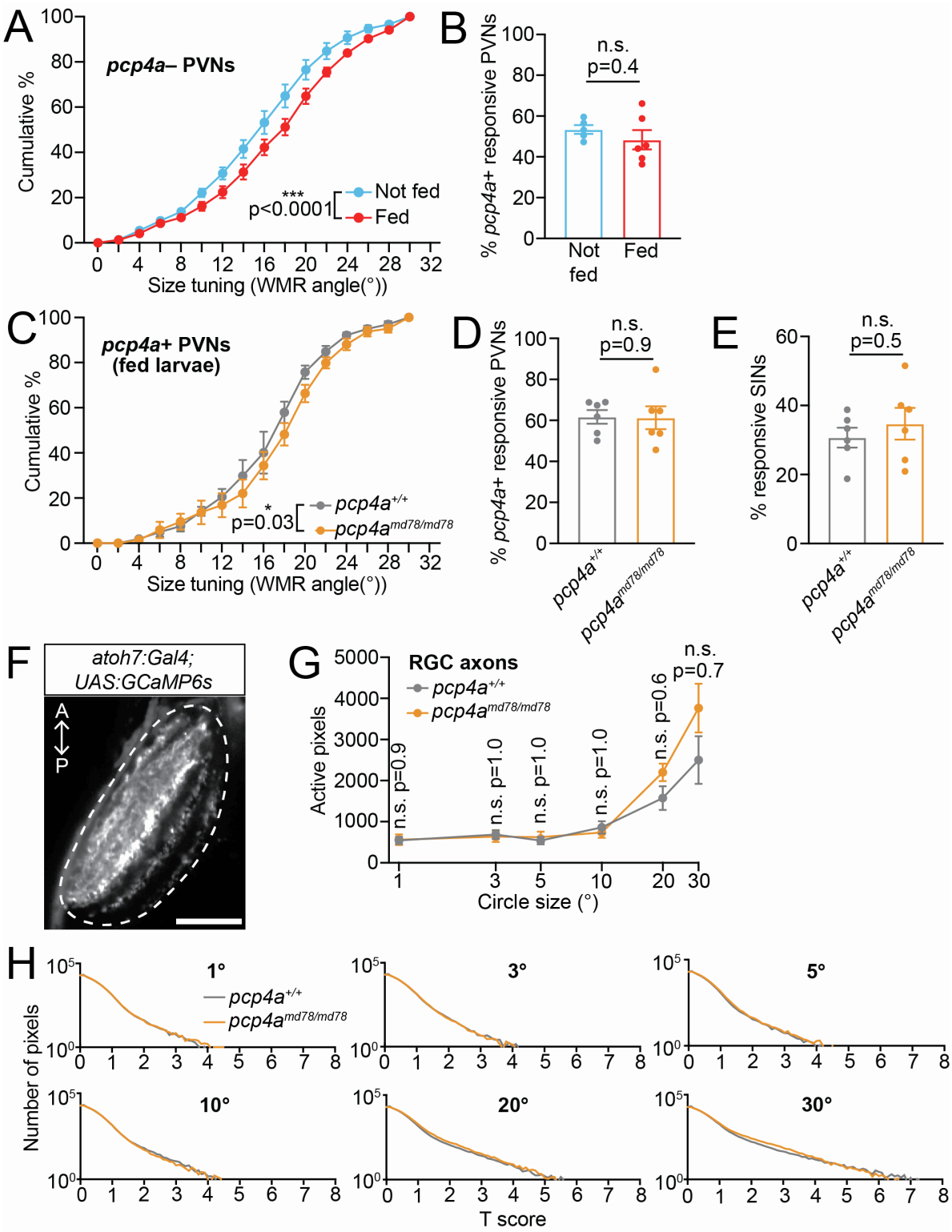

Figure S4. Food intake modifies response properties of *pcp4a*– PVNS but not number of responsive PVNs. The *pcp4a*^{md78} mutation has only a small effect on size tuning of PVNs in fed larvae, and does not alter number of responsive tectal neurons or responses of RGC axons to visual stimuli. Related to Figure 3. **A.** Graph depicting cumulative percentages of WMR angles of *pcp4a*– PVNs in food-deprived and fed 7 dpf *elavl3:H2B-GCaMP6s* larvae. n_{fed} = 6 fish, $n_{not\text{-}fed}$ = 5 fish. *** $p < 0.0001$, two-way ANOVA. **B.** Bar graph depicting average numbers

of *pcp4a*+ PVNs responsive to visual stimuli in 7 dpf fed and not-fed *elavl3:H2B-GCaMP6s*. $n_{not\text{-}fed}$ = 5 larvae, n_{fed} = 6 larvae. n.s., not significant, two-tailed t test. **C.** Graph depicting cumulative percentages of WMR angles of *pcp4a*+ PVNs in fed 7 dpf *elavl3:H2B-GCaMP6s; pcp4a*$^{+/+}$ and *elavl3:H2B-GCaMP6s; pcp4a*$^{md78/md78}$ larvae. n = 5 fish per group. * p = 0.03, two-way ANOVA. **D.** Bar graph showing average numbers of *pcp4a*+ PVNs responsive to visual stimuli in unfed 7 dpf *elavl3:H2B-GCaMP6s; pcp4a*$^{+/+}$ and *elavl3:H2B-GCaMP6s; pcp4a*$^{md78/md78}$ larvae. $n_{pcp4a+/+}$ = 6 larvae, $n_{pcp4amd78/md78}$ = 6 larvae. n.s., not significant, two-tailed t test. **E.** Bar graph showing average number of SINs responsive to visual stimuli in 7 dpf *elavl3:H2B-GCaMP6s; pcp4a*$^{+/+}$ and *elavl3:H2B-GCaMP6s; pcp4a*$^{md78/md78}$ larvae. $n_{pcp4a+/+}$ = 6 larvae, $n_{pcp4amd78/md78}$ = 6 larvae. n.s., not significant, two-tailed t test. **F.** Confocal image showing the tectal neuropil, labeled by retinal ganglion cell axons, of a 7 dpf *atoh7:gal4; UAS:GCaMP6s* larva. The dashed white line marks the borders of the neuropil region. Scale bar, 50 μm. A and P indicate anterior and posterior directions, respectively. **G.** Graph showing average numbers of active pixels in RGC axons of food-deprived 7 dpf *atoh7:gal4; UAS:GCaMP6s; pcp4a*$^{+/+}$ and *atoh7:gal4; UAS:GCaMP6s; pcp4a*$^{md78/md78}$ larvae in response to visual stimuli of different sizes. $n_{pcp4a+/+}$ = 14 larvae, $n_{pcp4amd78/md78}$ = 9 larvae. n.s., not significant, two-tailed t test with Bonferroni-Holm correction. **H.** Graphs depicting distribution of T scores obtained with the pixel-wise analysis based on a regression model to analyze responses of RGC axons to visual stimuli of different sizes in 7 dpf *atoh7:gal4; UAS:GCaMP6s; pcp4a*$^{+/+}$ and *atoh7:gal4; UAS:GCaMP6s; pcp4a*$^{md78/md78}$ larvae (see Materials and Methods for details). $n_{pcp4a+/+}$ = 14 larvae, $n_{pcp4amd78/md78}$ = 9 larvae. Data in (A – E, G) are presented as mean ± standard error of the mean.

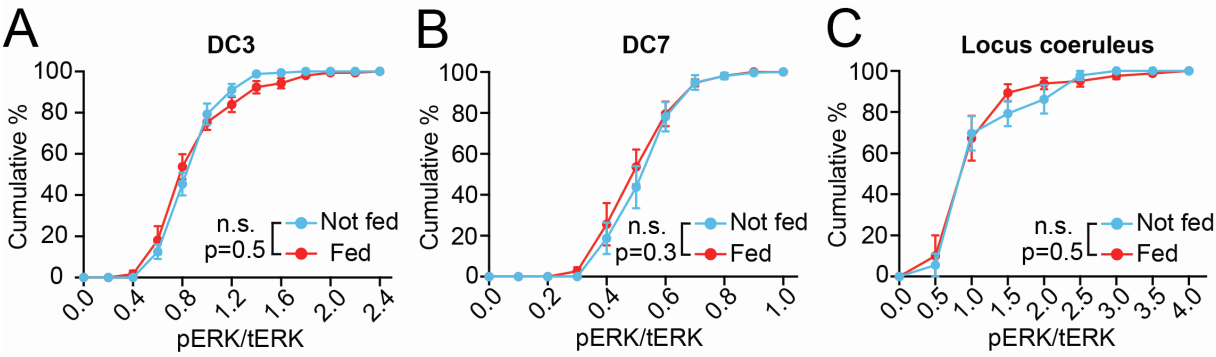

Figure S5. Food intake does not alter activity of DC3 and DC7 dopaminergic neurons, and noradrenergic neurons of the locus coeruleus. Related to Figure 4. **A – C.** Graphs showing cumulative percentages of pERK/tERK values in dopaminergic neurons in the DC3 (A) and DC7 (B) clusters, and in noradrenergic neurons in the locus coeruleus (C) in fed or food-deprived 7 dpf *th:gal4-VP16; UAS:EGFP-CAAX* larvae. $n_{not\text{-}fed} = 9$ larvae, $n_{fed} = 10$ larvae. n.s., not significant, two-way ANOVA. Data are shown as mean ± standard error of the mean.

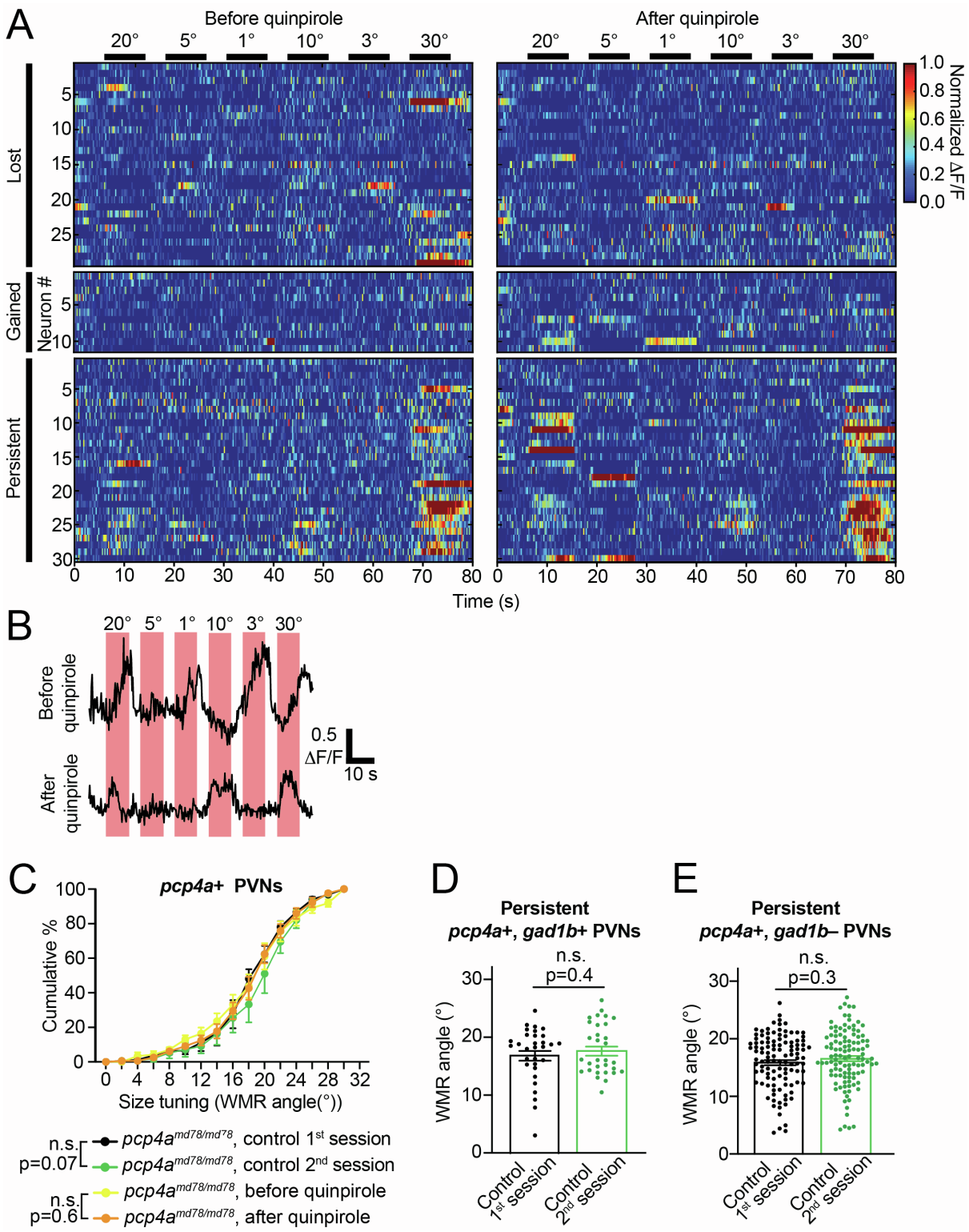

Figure S6. Responses to visual stimuli of *pcp4a*+ PVNs before and after treatment with quinpirole. Related to Figure 5 and 6. **A.** Heatmap showing activity of lost, gained and persistent *pcp4a*+ PVNs in response to visual stimuli of different sizes in a 7 dpf *elavl3:H2B-GCaMP6s* larvae before and after treatment with quinpirole. **B.** Examples of traces of a persistent *pcp4a*+ PVNs which responded to small and large visual stimuli before treatment with quinpirole, and only to large ones after. **C.** Graph showing cumulative percentages of

WMR angles of *pcp4a*+ PVNs in unfed 7 dpf *pcp4a*$^{md78/md78}$; *elavl3:H2B-GCaMP6s* larvae before and after three hours treatment with quinpirole and in untreated controls kept in agarose for the same duration of the drug treatment. $n_{control}$ = 3 fish, $n_{quinpirole}$ = 4 fish. n.s., not significant, two-way ANOVA. **D, E.** Graphs depicting WMR angles of *pcp4a*+/*gad1b*+ (D) or *pcp4a*+/*gad1b*– (E) PVNs in the tecta of 7 dpf *elavl3:H2B-GCaMP6s* larvae before (1st session) or after three hours of permanence in agarose (2nd session) without drug treatment. *pcp4a*+/*gad1b*+: 31 neurons from 4 fish, *pcp4a+/gad1b–:* 110 neurons from 4 fish. n.s., not significant, paired t test. Data are shown as mean ± standard error of the mean. Individual data points are also shown.